INVESTIGATION OF THE RELATIONSHIP BETWEEN FLUID-TURBULENCE CHARACTERISTICS AND THE DIFFUSION OF SOLID PARTICLES

A THESIS

Presented to

the Faculty of the Graduate Division

By

Richard Cleveland Farmer

In Partial Fulfillment

of the Requirements for the Degree

Doctor of Philosophy in Chemical Engineering

Georgia Institute of Technology

March 1962

"In presenting the dissertation as a partial fulfillment of the requirements for an advanced degree from the Georgia Institute of Technology, I agree that the Library of the Institution shall make it available for inspection and circulation in accordance with its regulations governing materials of this type. I agree that permission to copy from, or to publish from, this dissertation may be granted by the professor under whose direction it was written, or, in his absence, by the dean of the Graduate Division when such copying or publication is solely for scholarly purposes and does not involve potential financial gain. It is understood that any copying from, or publication of, this dissertation which involves potential financial gain will not be allowed without written permission.

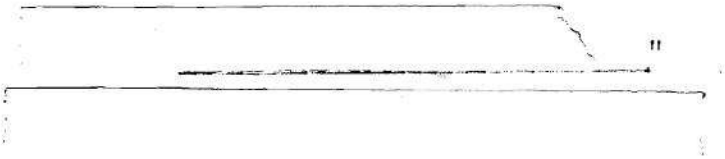

3 8
12 R

INVESTIGATION OF THE RELATIONSHIP BETWEEN FLUID-TURBULENCE CHARACTERISTICS AND THE DIFFUSION OF SOLID PARTICLES

APPROVED:

Date Approved by the Chairman: May 25, 1962

ACKNOWLEDGMENTS

The author wishes to express his appreciation to Dr. M. R. Carstens for his suggestion of the problem and his advice and guidance, to Dr. H. C. Ward for his encouragement and interest, to Mr. Ed Flynt for the conception of the timer, to Mr. Homer Bates for his ingenuity in the construction of the equipment, to Dr. Earl McDaniel for his generosity in the loan of radiation-sensing equipment.

The author is grateful to the National Science Foundation for their interest and financial support of this project.

TABLE OF CONTENTS

		Page
ACKNOWLEDGMENTS		iii
LIST OF TABLES		v
LIST OF FIGURES		vi
NOMENCLATURE		viii
SUMMARY		xii
CHAPTER		
I.	INTRODUCTION	1
II.	EDDY DIFFUSION OF FLUID PARTICLES IN A TURBULENT FIELD	3
III.	EDDY DIFFUSION OF FOREIGN PARTICLES SUSPENDED IN A TURBULENT FIELD	34
IV.	CONCLUSIONS AND RECOMMENDATIONS	66
APPENDIX		
I.	ELECTRONIC SYSTEMS	69
II.	PHOTOCELL CALIBRATION	73
III.	FLUID-DIFFUSION DATA	77
IV.	PHOTOMICROGRAPH AND FALL VELOCITY OF BEADS	91
V.	PARTICLE-DIFFUSION DATA	92
LITERATURE CITED		109

LIST OF TABLES

Table		Page
1.	Fluid-Diffusion Data, Run 13	19
2.	Summary of Data-Eddy Diffusion of Fluid	23
3.	Values of $0.0413(u^*/U)^{1/3}$ for a Smooth Pipe	24
4.	Particle-Diffusion Data, Runs U and W	41
5.	Summary of Data-Eddy Diffusion of Beads	45
6.	Photospectrometer Calibration	74
7.	Photocell Calibration	74
8.	Fluid-Diffusion Data	78
9.	Particle-Diffusion Data	93

LIST OF FIGURES

Figure		Page
1.	Diffusion Chamber	6
2.	Nozzles	7
3.	Turbulence-Generator Pump	8
4.	Pump Controls	11
5.	Spring-Mass System	12
6.	Recorder	13
7.	Typical Strip-Chart Record	18
8.	Fluid Diffusion, Run 13	22
9.	Flow Patterns from the Jets	26
10.	Relationship Between the Fluid-Diffusion Coefficient and the Product of Amplitude and Frequency	33
11.	Radiation Sensing and Recording System	37
12.	Raw Data from Runs U and W	42
13.	Reduced Data from Runs U and W	44
14.	Relation Between the Particle-Diffusion Coefficient and the Product of Amplitude and Frequency	46
15.	Plane of Concentration Sensing Not Horizontal	48
16.	Cross Sections Through Collimator	50
17.	Effect of Sediment Traps upon Count Rate	54
18.	Wiring Diagram of Timer	70
19.	Differential-Transformer Circuit	71
20.	Photocell Balancing Circuit	72

Figure		Page
21.	Photospectrometer Calibration	75
22.	Photocell Calibration	76
23.	Microphotograph of Beads (50x)	91

NOMENCLATURE

a	position of pump piston, ft
a_o	pump stroke, in
A	cross sectional area normal to fluid velocity, ft^2
A_n	cross sectional area of a nozzle, ft^2
A_p	cross sectional area of pump piston, ft^2
A^*	cross sectional area of a particle normal to fluid velocity, ft^2
b	distance between horizontal rows of nozzles, ft
c	concentration of diffusing substance, $slugs/ft^3$
c_o, c_1, c_2	direct and reflected concentrations, $slugs/ft^3$
C	count rate from radioactive beads, counts/min
C_o, C_1, C_2	particular count rates, counts/min
C_c	contraction coefficient for a nozzle, dimensionless
C_d	drag coefficient for spheres, dimensionless
C_{d_s}	drag coefficient for spheres settling in a still fluid, dimensionless
C_v	viscous damping coefficient, lb-sec/ft
CR	chart reading, cm
d	distance from dye source to sensing element, ft
d_o, d_1, d_2	direct and reflected distances from dye source to sensing element, ft
D	eddy-diffusion coefficient, ft^2/sec
D_f	fluid eddy-diffusion coefficient, ft^2/sec

D_j	contracted-jet diameter, ft
D_p	particle eddy-diffusion coefficient, ft^2/sec
D_t	particle eddy-diffusion coefficient in sediment traps, ft^2/sec
e	energy level of detected radiation, dial units
E	energy dissipation rate per unit mass, ft-lbs/slug-sec
E_o	energy of matter within the control volume, ft-lbs
f	pump (or system) frequency, cps
F	rate of transport, $slugs/ft^2$-sec
I	detected emission rate, counts/min
k	recorder chart speed, cm/sec
k_1	generated ratiation rate per element of depth per unit of radiating surface, $counts/in^3$-min
k_m	virtual mass coefficient, dimensionless
K_o	constant defined by Orlob's diffusion equation, dimensionless
K, K_1	constants defined by unsteady-state diffusion equation, dimensionless
K*	product of fall velocity and square root of drag coefficient, ft/sec
$\ddot{\ell}$, $\dot{\ell}$, ℓ	fluid acceleration, velocity, and displacement; ft^2/sec, ft/sec, ft
$\mathscr{L}$	Lagrangian mean eddy size, ft
L	strip-chart length, cm, proportional to elapsed time
M	displaced fluid mass, slugs
M_o	particle mass, slugs

n	number of nozzles in the diffusion chamber, dimensionless
N	fraction of particles whose motion was restrained by the system boundaries, dimensionless
p	pressure, lbs/ft^2
r	pipe radius, ft
R	count rate expressed as: no. of 64 counts-no. of unit counts/no. of min
t	time, sec
T	period of pump, sec
u	fluid velocity, ft/sec
u^*	shear velocity, ft/sec
u_r	relative velocity between fluid and particle, ft/sec
U	mean fluid velocity, ft/sec
$\forall$	volume of diffusion chamber, ft^3
V_p	pump piston velocity, ft/sec
w	particle settling velocity, ft/sec
w_r	particle settling velocity of particles restrained by system boundaries, ft/sec
w_s	particle settling velocity in a still fluid, ft/sec
$\ddot{x}$, $\dot{x}$, x	particle acceleration, velocity, and displacement; ft/sec^2, ft/sec, ft
x_o	particle amplitude in pulsating field, ft
y	dimension normal to the nozzle studded face of the diffusion chamber, ft
y_1	a particular y, ft
z	elevation, ft

z_o, z_1, z_2	particular elevations, ft
α	angle of tilt of the diffusion chamber, radians
γ	specific weight of fluid, lbs/ft^3
ϕ	phase angle between particle and fluid, radians
ρ	fluid density, slugs/ft^3
ρ_s	particle density, slugs/ft^3
ω	pump (or system) frequency, sec^{-1}

SUBSCRIPTS, UNLESS DEFINED ABOVE

c	central region of radiating surface
f	side of diffusion chamber furthest from radiation sensor
F	fringe region of radiating surface
o	conditions within the diffusion chamber
j	conditions at the control surface
n	side of the diffusion chamber nearest to the radiation sensor
U and W	values for a particular run

SUPERSCRIPTS, UNLESS DEFINED ABOVE

*	a particular position
-	mean value

SUMMARY

The transport of foreign particles in a fluid medium is a common physical phenomenon. Examples are suspensions of sediment in streams, dust and mist in the atmosphere, droplets in fuel-injection systems, vapor bubbles in distillation columns, slurries, and fluidized beds of catalysts. These examples may be considered in two categories: the first is that in which the fluid is made up primarily of the particles (slurries and fluidized beds), and the second is that in which the fluid is a dilute suspension of small particles (the remaining examples). The motion of the particles in a dilute suspension may be considered eddy diffusive, being characterized by transport of the particles by the turbulent fluctuating velocities of the fluid in a direction normal to the direction of average flow. The concentrated suspensions are further complicated by the collision and collusion of the particles; such flows can be treated as non-Newtonian or as special cases, as for example in fluidized beds of catalysts. This investigation was a study of the eddy-diffusion problem.

The understanding of particle transport requires extensive knowledge, which can be classified as an adequate description of the particles, the turbulent motion, and the relationship between the fluid motion and the particle motion. This investigation was a study of the relative motion of the fluid and particles. For a specific type of particle and of turbulence, the motion of the fluid and particles was defined in terms of mass-transport properties.

The transport of foreign and fluid particles can be expected to differ because of their different inertial reaction to movement. This effect was investigated by performing two experiments in the same turbulent environments. One of the experiments determined the eddy diffusion of the turbulent fluid; the other, the eddy diffusion of small spherical particles in the fluid.

The eddy diffusion of turbulent fluid was observed by injecting dyed fluid into a turbulent field and measuring the diffusion of the dye. The observation was performed in such a manner that the unsteady-state diffusion equation of the heat-conduction type correctly described the spread of the dyed material. In other words, the diffusion coefficient completely described the transport process. The turbulent field was generated artificially by periodically pumping water through a closed chamber. The turbulence was homogeneous in the vertical direction, as was evidenced by the constancy of the diffusion coefficients measured in this direction. The pump frequency and stroke, which were varied to change the turbulence characteristics, as well as the geometry of the system, completely defined the turbulent motion, although not in the more common parameters of scale and intensity. The oscillation frequency, f (cycles per second), was varied from two to five, and the maximum stroke, a_o (inches), from one to three and one-half. The diffusion coefficients, D_f (square feet per second), for the water were found to be well represented by the equation:

$$D_f = 0.0136\ E^{1/3}\ \ell^{4/3} \qquad (a)$$

which was presented by Orlob (Journal of the Hydraulics Division, Proceedings of the American Society of Civil Engineers, 85, No. HY 9, 75-101, 1959) for statistically homogeneous flow in broad open channels. The energy dissipation rate, E, was calculated by means of an energy balance on the diffusion chamber. The Lagrangian mean eddy size, ℓ , was derived by a rational consideration of the flow pattern in the generator; since the geometry was invariant, the eddy size was constant. Written in terms of the independent variables of the system, equation (a) becomes:

$$D_f = 3.9(10)^{-4} a_o f \qquad (b)$$

in which a_o and f are the pump amplitude and frequency, respectively. Equation (b) is applicable to the experimentally determined results of these experiments.

The eddy diffusion of foreign particles suspended in a fluid was measured by tagging ion-exchange resin beads with radioactive cesium and measuring the count-rate at various elevations in the fluid. The resin beads were spherical in shape, uniform in size, and of constant density. Sphericity was verified and size measured from photomicrographs; bead density was determined from fall-velocity measurements. The particles were 0.0117 inches in diameter and 2.54 slugs per cubic foot in density. The same artificial turbulence generator was used to create the turbulent field. The equilibrium state of the normal transport of the particles was described by the steady-state diffusion equation of the heat-conduction type from which the diffusion coefficient was calculated. The

diffusion coefficient of particles D_p was reasonably characterized by the equation

$$D_p = 2.6\,(10)^{-4}\; a_o f \qquad (c)$$

After numerous possibilities were reviewed, it was concluded that early transition to turbulence in the boundary layer surrounding a particle is the most probable reason for the reduction in diffusion coefficients. A simplified theoretical analysis in which a completely turbulent boundary layer was assumed indicates that this explanation is reasonable.

Probably the most significant result of this experiment is the additional confirmation of the generalization that

$$D \propto E^{1/3} \mathcal{L}^{4/3} \qquad (d)$$

in which E is rate of energy dissipation per unit mass and $\mathcal{L}$ is the Lagrangian mean eddy size. The development of this generalization can be traced to the work of Richardson, Kolmogoroff, Taylor, and Batchelor, but Orlob has most clearly stated the principle. The principle previously has been shown to be valid in uniform open channel flow (Orlob) and in pipe flow (Taylor).

CHAPTER I

INTRODUCTION

One of the important properties of a turbulent stream is its ability to suspend and transport foreign particles. This ability is manifested in sediment transport in rivers, vapor bubbles in distillation columns, liquid droplet suspensions in fuel injection systems, and radioactive fallout from the atmosphere. These examples are all dilute suspensions of particles, which may be considered eddy-diffusion processes. An eddy-diffusion process is characterized by lateral transport of matter due to the turbulent fluctuations of a fluid. When the suspension is so concentrated that the particles collide or coalesce, the representation by the diffusion process is no longer valid; examples of this are flows of slurries and fluidized beds of catalyst. The concentrated suspensions may be considered as non-Newtonian fluids or as fluids composed entirely of particles. This investigation was a study of the eddy-diffusion process.

Eddy-diffusion processes have been investigated in many different types of flow systems. Sediment transport in open and closed channel flow (Ismail /1/ and Vanoni /2/), fuel injection systems (Longwell and Weiss /3/), and deposition of particles from air on the walls of ducts (Freilander and Johnstone /4/) are illustrations of these investigations. Mathematically such systems have been described by Tchen /5/, Peskin /6/, Lumley /7/, Corrsin and Lumley /8/. Hinze /9/ reviews the mathematics and

literature very excellently in his book. The most comprehensive overall survey has been prepared by Torobin and Gauvin /10/.

Qualitatively these studies complement each other, but, because of the complex nature of turbulence, there is no quantitative relationship between the different types of experiments.

The purpose of this investigation was to determine the relationship between the eddy diffusion of a fluid in turbulent motion and the eddy diffusion of foreign particles suspended in the fluid. Two experiments were performed in the same turbulent field; one to determine the fluid diffusion and the other, the particle diffusion. The turbulent field and the particles were chosen so that they could be uniquely defined and easily described. The experiments were designed so that the eddy diffusion coefficients could be used to describe the diffusion processes; hence, the eddy diffusion coefficients of fluid and particles, when compared, yielded the desired relationship. The turbulent field was varied so that the generality of this relationship was established and the dependence of the diffusion on the turbulence characteristics was observed.

The two experiments will be described separately; the conclusions from them will be presented jointly.

CHAPTER II

EDDY DIFFUSION OF FLUID PARTICLES IN A TURBULENT FIELD

The eddy diffusion of fluid particles was investigated experimentally. The investigation consisted of observing the spread of a dye of approximately the same density and viscosity as the fluid in an artificially generated field of turbulence and of using a mathematical model to describe these observations.

The one-dimensional unsteady diffusion equation of the heat-conduction type

$$\frac{\partial c}{\partial t} = - D_f \frac{\partial^2 c}{\partial z^2} \tag{1}$$

was chosen as the mathematical model. If a given amount of material is injected into an infinite rectangular diffusion chamber on the plane, $z = 0$, and at time, $t = 0$, eq. (1) can be solved provided that the diffusion coefficient, D_f, is constant and no material is transferred through the walls of the diffusion chamber.

$$c \propto \frac{1}{\sqrt{D_f t}} e^{-z^2/4 D_f t} \tag{2}$$

The diffusion coefficient, in this case an eddy-diffusion coefficient, is a complete measure of the eddy diffusion.

The mathematical model was duplicated experimentally by the instantaneous injection of dye at position z = 0 and time t = 0 and by measurement of the concentration of dye at a fixed position of z as time t varied. The diffusion coefficient, D_f, was calculated by means of eq. (2). In this case the diffusion equation is applied to diffusion in homogeneous turbulence. The diffusion coefficient is a measure of the intensity of both turbulent and molecular diffusion. However, the contribution of molecular diffusion is negligible in the experiments reported herein.

The turbulent field was of necessity a simple one so that the relative motion of the fluid and foreign particles could be completely determined. Rouse /11/ built an artificial turbulence generator which produced such a simplified field. His generator consisted of a periodically agitated lattice in a container of water; the turbulence was varied directly by changing the frequency of agitation. Rouse used this device for the determination of the diffusion characteristics of several sizes of small sand particles. Rouse assumed a constant diffusion coefficient in this system implying that the turbulence created was homogeneous. In Holland, Bouwman /12/ duplicated Rouse's experiments with slight changes in the agitating bars. Bouwman's equipment was designed so that the frequency, amplitude, and geometry could be varied; but this study was limited by the shortage of materials brought about by World War II.

The turbulence generator used in the present study employed liquid jets rather than mechanical agitators. This device had the advantage of producing a volume of turbulent fluid free from obstructions such as mixing bars. The amplitude and frequency of the pump were changed to vary the turbulence characteristics.

The details of this investigation and the mathematical model employed will be discussed in the subsequent sections of this chapter.

Equipment

The eddy diffusion of fluid was studied in a synthetically produced field of turbulence by observing the motion of injected dye.

The synthetic field of turbulence was generated in a closed diffusion chamber by the influx and efflux of water which was energized by a reciprocating pump. This chamber is shown in Fig. 1. The diffusion chamber was a box 22.4 inches in length and six inches by one inch in cross section. One of the 6-in sides was studded with seventy-two 0.190-in diameter holes that served as nozzles as shown in Fig. 2. The top, bottom, and three sides of the box were made of plastic; the fourth side which contained the holes was brass. The top and bottom contained ports to which a pressurized water-storage tank was connected. Pressurization prevented cavitation at the pump. The chamber was mounted on a pivot, such that if the brass side were horizontal, there was no effect of gravity normal to the jet flow into and out of the chamber, and if the brass side were vertical, the gravity effect was at a maximum. Nipples, one-quarter inch by one inch, connected the nozzles of the brass plate to glass sediment traps. The glass sediment traps were one inch in diameter by six inches in length and were dished and were reduced to one-quarter inch at the ends. One-quarter inch by thirty-inch Jessal plastic tubing connected the sediment traps to the two thirty-six outlet manifolds. Alternate horizontal rows of nozzles were connected to one of the manifolds; the other nozzles to the other manifold. The pump and the manifolds are shown in Fig. 3. The copper manifolds above the pump were eight-in in

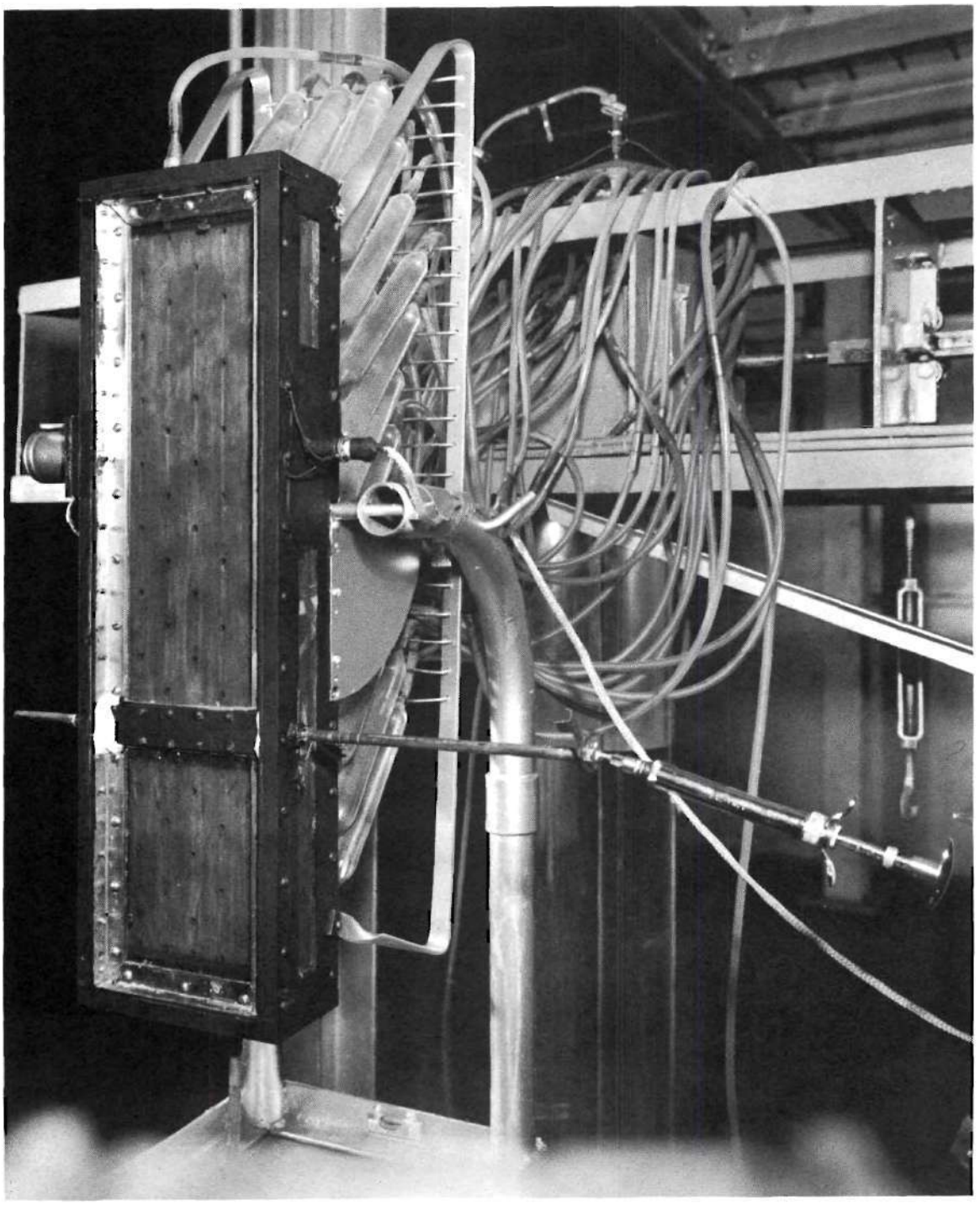

Figure 1. Diffusion Chamber.

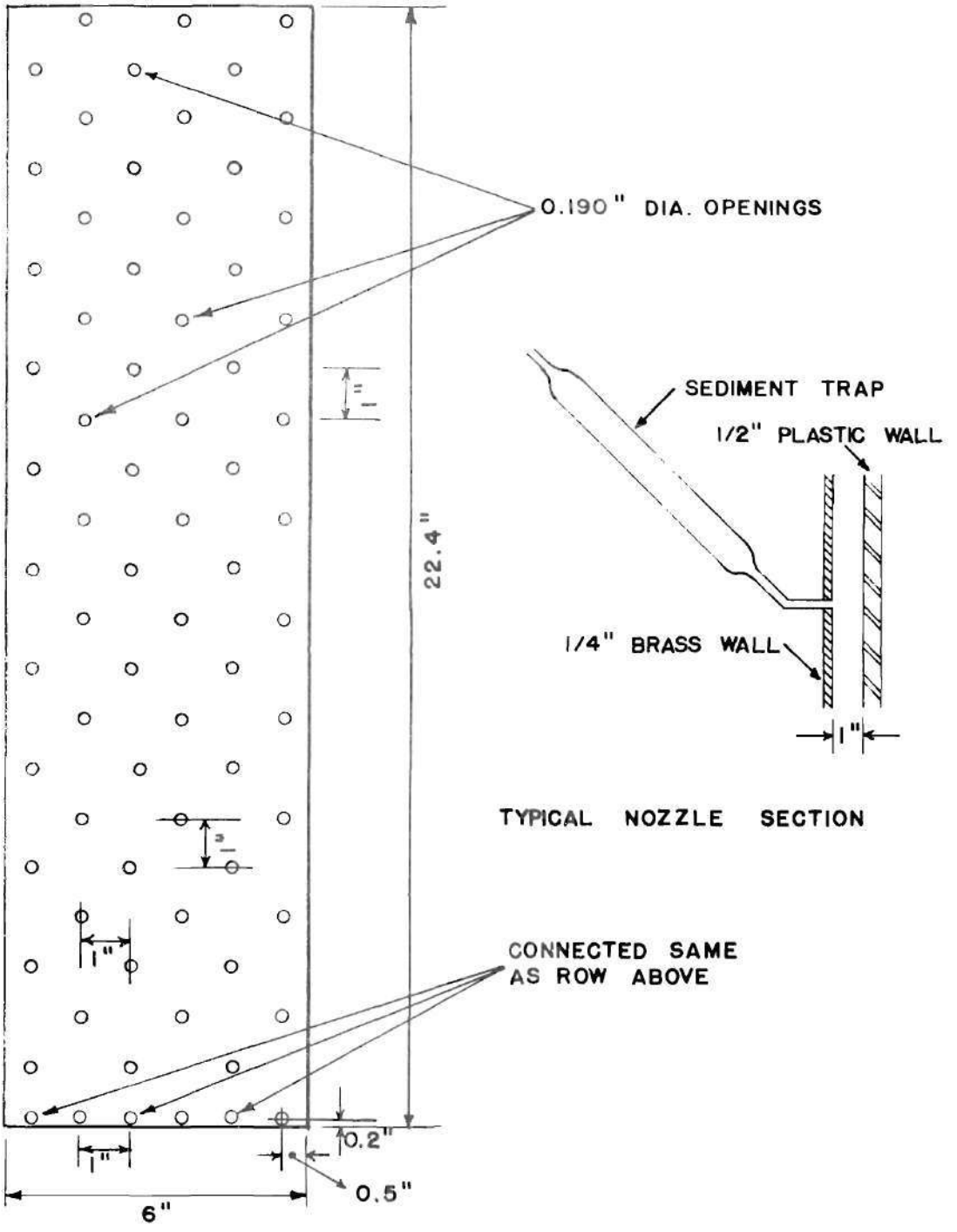

Figure 2. Nozzles.

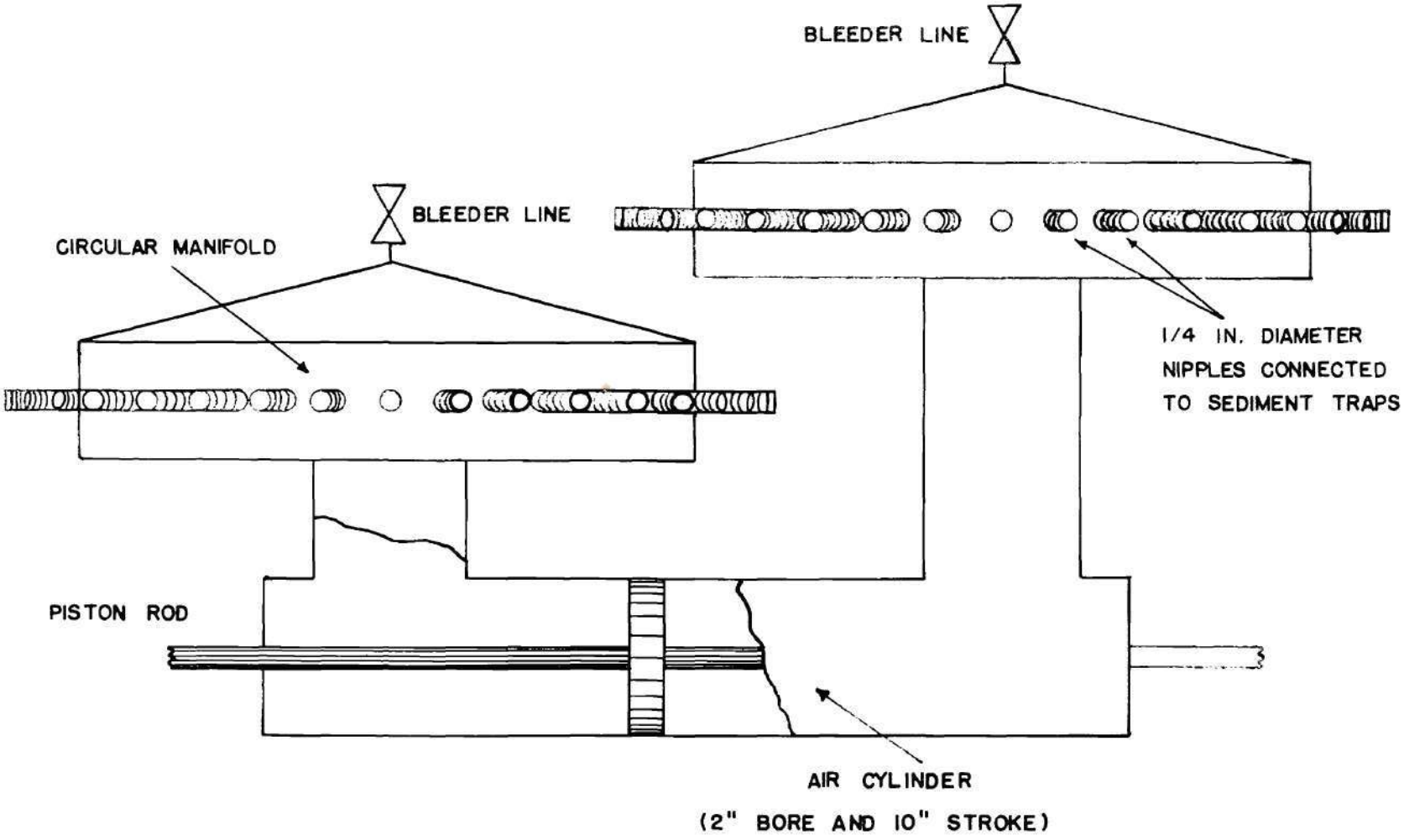

Figure 3. Turbulence-Generator Pump.

diameter. The conical tops and air bleeds on the manifolds facilitated removal of entrapped air in filling the system. The manifolds were connected to the pump by two-inch diameter copper tubing. The pump was made from a Bellows Power Dome Series 2010 FDE air cylinder. The diameter of the piston rod was five-eighths of an inch. The pump was submerged in a water tank to prevent suction of air into the system; a thermometer in this tank was used to measure the system temperature. This completes the description of the fluid-containing sections of the turbulence generator.

The power supply and controls for actuating the pump piston comprised the remainder of the generator. The power supply consisted of an air-drive unit which converted a compressed air source into periodic impulses to the pump piston. Air from a 175-pound-per-square-inch source flowed through a filter, Bellows Model F-375; regulator, Bellows Model R-375; and lubricator, Bellows Model L-375, into a surge tank. A second regulator was used in the air inlet line to provide static pressure for the fluid system. Air was taken from the surge tank through an electronically controlled solenoid valve to either of the two air cylinders, Bellows Double Acting Han-D-Air Cylinder, DA-4, which were mounted on either end of the piston rod. The solenoid valve operated so that air was in one side or the other of the air cylinders at all times; hence, the pump piston was being forced in one direction or the other at all times. The electronic timing unit controlled a duration of the force. The pressure in the surge tank controlled the magnitude of the force. The frequency and amplitude of the pump piston were, therefore, determined by the pressure regulator and electronic timer. The timer produced

a step output to one of the circuits in the solenoid valve for one-half cycle, then a step to the other circuit for one-half cycle. A wiring diagram of the timer is presented in Appendix I.

The mass and spring system was employed in order to obtain harmonic motion of the piston pump. A one-inch square steel bar, bedded in ball-bearing traces, was connected in series to the pump piston and air cylinders. One-quarter-inch thick slotted iron plates were clamped over this bar in order to achieve an adjustable mass. Coil springs (4 - 16 in number) were attached to the bar. However, since the life of the coil springs was too short, the coil springs were replaced with a three-layer automobile spring. The laminated spring consisted of one-quarter in by three-in spring-steel plates which were twenty-four inches in length. This cantilevered spring was adjustable in length in order to provide a variation of the spring constant. Position sensing was accomplished by connecting an Atcotran Differential Transformer, Class 6205B, in series with the pump piston. The output of the transformer was proportional to the position of the pump piston. A signal converter modified the signal before it was sent to an AC amplifier, Sanborn Model 64-500A, thence into a recorder, Sanborn Model 60-1300. The circuit diagram of the differential-transformer circuit is shown in Fig. 19 (Appendix I).

Figs. 4, 5 and 6 show the pump controls, spring-mass system, and recorder, respectively.

The dye was injected into the diffusion column. The dye injector was mounted in the plastic face opposite the brass plate. A 0.025-inch horizontal slot was cut in the plastic side. The slot was connected tangentially to a hole which accommodated a five-sixteenths inch diameter

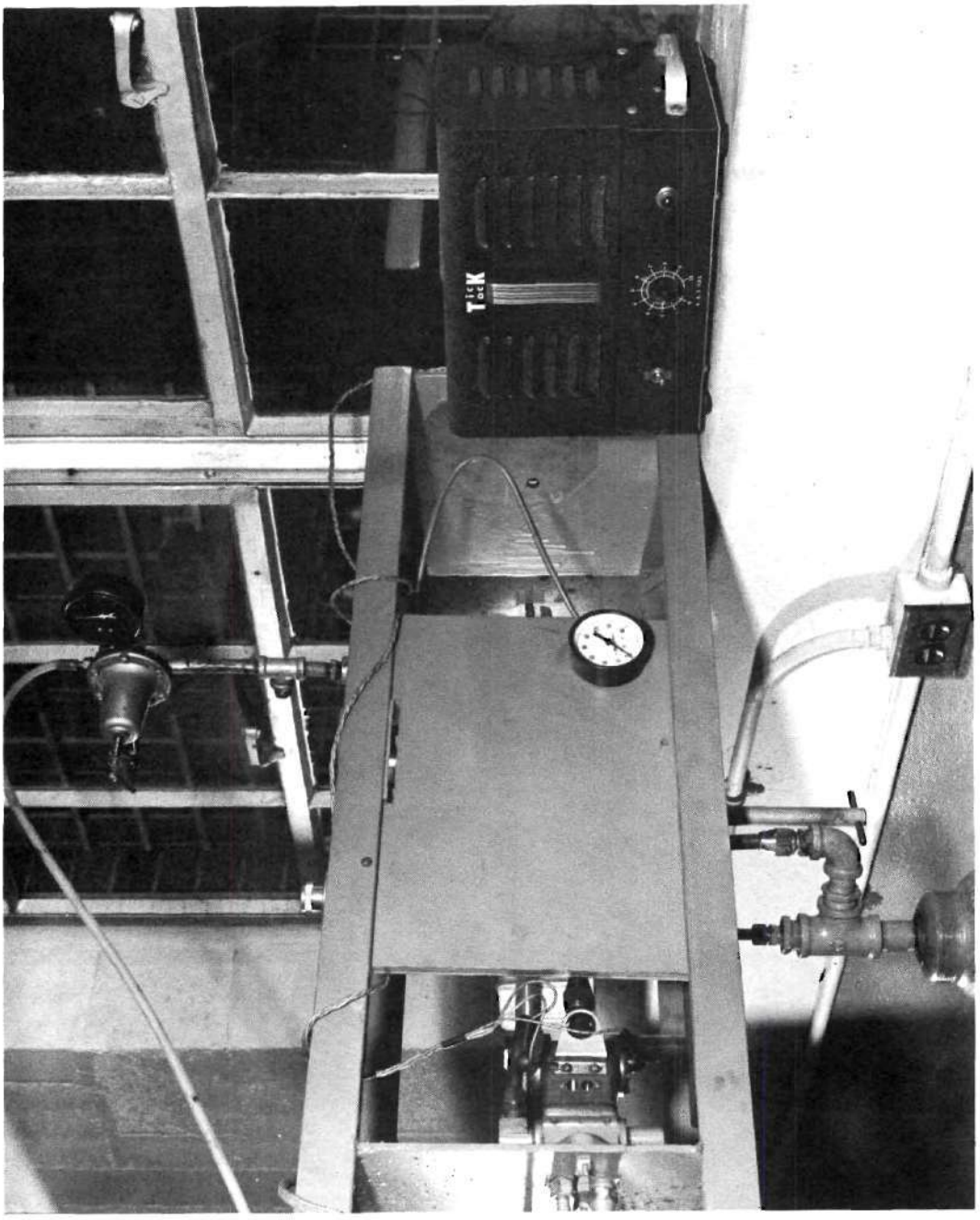

Figure 4. Pump Controls.

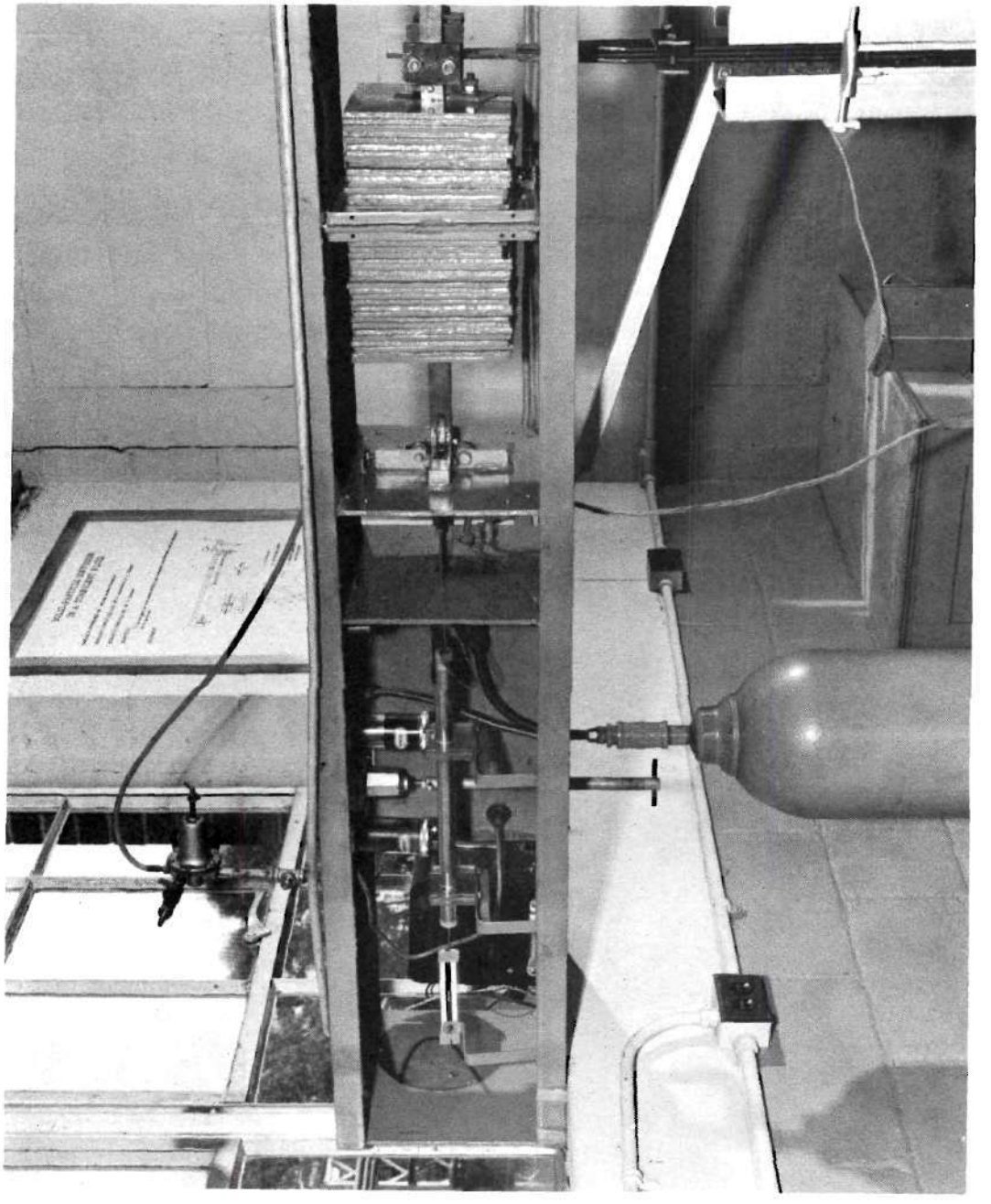

Figure 5. Spring-Mass System.

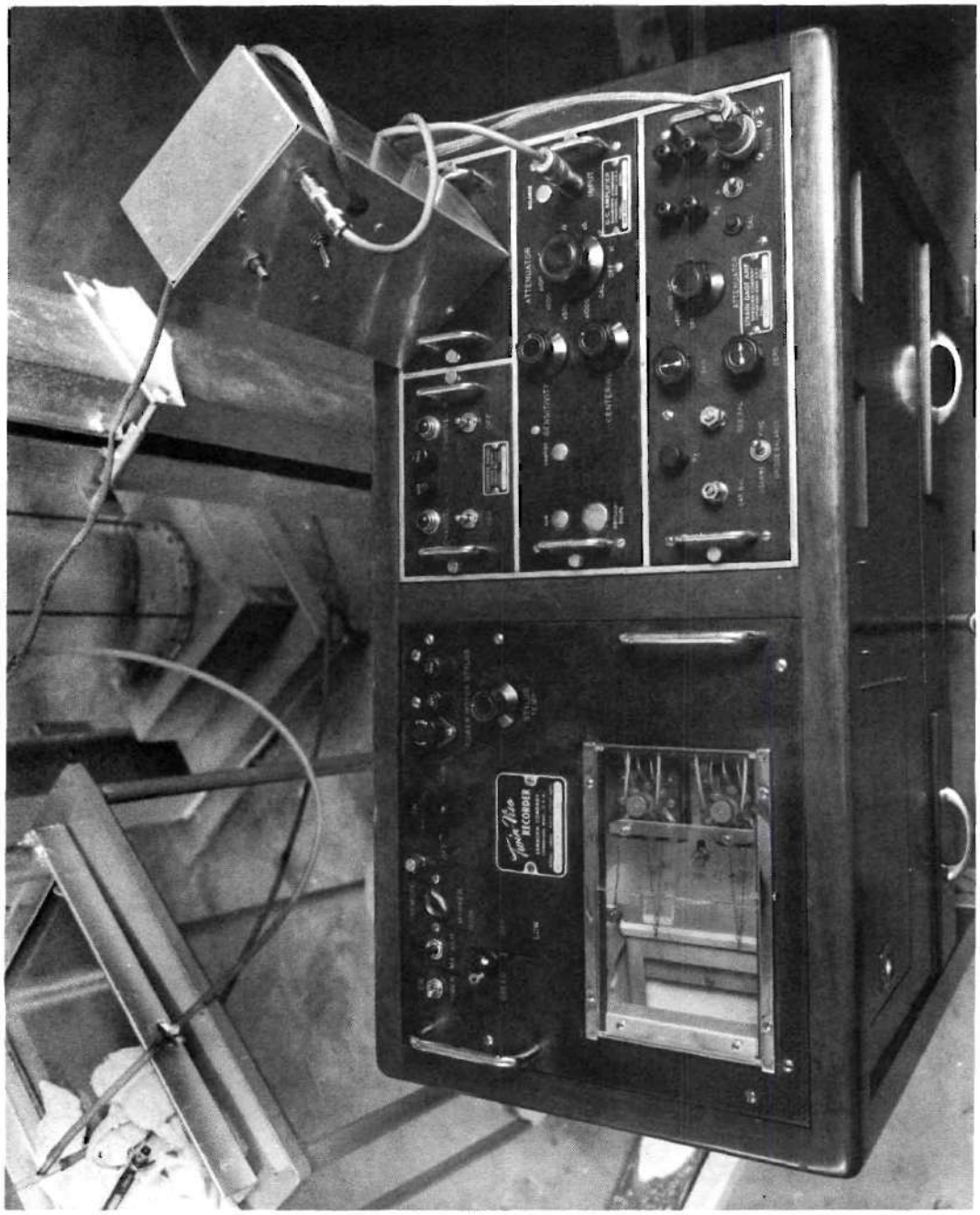

Figure 6. Recorder.

bar. The bar was drilled axially and numerous times along one tangent. The bar was rotated to align the side holes with the slot in the chamber. Dye was injected into the axial hole by means of a hypodermic syringe. The rod was twice as long as the slot so that it could be partially withdrawn to close the slot. The dye injector was located 7.00 inches from the bottom of the chamber as shown in Fig. 1.

Dye concentration was determined by measuring light transmission through the column. The light source was the bright filament of a twelve-volt light. The selenium-sulfide photocell had a one-quarter inch diameter sensitive face and was located 8.31 inches from the dye injector. The photocell was placed in one leg of a parallel circuit as shown in Fig. 20 (Appendix I) in such a manner as to generate an opposing emf. The emf measured between two points of the parallel circuits was amplified and recorded by means of a Sanborn Model 64-300B amplifier and a Sanborn Model 60-1300 recorder. The circuits were initially balanced such that the sensed emf was zero with no light falling on the photocell. The photocell unit was calibrated by comparing the photocell-unit output to that of a Beckman Du photospectrometer with identical dye suspensions. In addition, dye suspensions of known concentration were tested for light transmission in the photospectrometer. Calibration data are presented in Appendix II.

Procedure During a Run

Fluid-diffusion coefficients were determined from measurements of the spread of dye within the chamber. The step-by-step procedure during a given run is as follows:

(a) The spring constant was adjusted. This adjustment consisted of attaching the proper number of coil springs depending upon the frequency of operation. In the later runs, the free length of cantilever spring was adjusted.

(b) Mass increments were fastened on the pump-drive shaft (Fig. 5). The number of mass increments placed on the oscillating drive shaft was a function of the frequency of operation. The exact number was established by observing the pump-drive motion record. Mass increments were added until the position-versus-time records were symmetrical rather than skewed.

(c) The position-sensing unit was calibrated by moving the drive shaft two inches. The amplifier of the recorder was then adjusted such that 1 cm chart deflection was equal to 1 in of shaft movement.

(d) A static pressure of 10 psi was applied to the diffusion column in order to prevent cavitation at the pump.

(e) The bleeder lines on top of the pump manifolds (Fig. 3) were opened slightly. Dissolved and entrained air in the water tended to be separated from the water on the suction stroke of the pump. This separated air was quickly removed through the bleeder lines. The loss of water was negligible.

(f) The timer (Fig. 4) which switched the solenoid valves was started at the desired frequency.

(g) The pressure regulator preceding the surge tank was adjusted until the desired amplitude of pump motion was achieved.

(h) Water temperature was determined.

(i) The photocell unit was calibrated and placed in operation.

The recorder zero was established with the light beam passing through the clear water and column. A filter was then placed in front of the light beam and the recorder amplifier was adjusted for a 2.5 cm deflection on the recorder chart.

(j) Water suspensions of the Dupont Ponsol DABP dye were injected slowly into the diffusion column. Rapid injection of the dye resulted in currents within the column which, in turn, resulted in exaggerated diffusion. This difficulty was avoided by injecting the dye steadily for a period of approximately 4 seconds. Timing marks were impressed on the recorder chart at the beginning and end of the dye injection period.

(k) The run was terminated when the recorder-stylus deflection of the photocell unit equalled the strip-chart width. Inasmuch as the data were to be analyzed by means of eq. (2), the terminal time could also have been established by the applicability of eq. (2). Equation (2) was derived for an infinitely long diffusion column but was applied to a column of finite length. The appropriate mathematical model can be formulated by placing two fictitious dye sources along the infinite column with a spacing equal to twice the distance from the real source to the end of the column. By this procedure the total amount of dye within the finite column remains constant. The concentration at the sensing element, photocell, is then simply the sum of the concentrations from the real source and two fictitious sources.

$$C = C_0 + C_1 + C_2$$

or

$$c \propto e^{-d_0^2/4D_f t} + e^{-d_1^2/4D_f t} + e^{-d_2^2/4D_f t}$$

in which the d's are the distance from the appropriate source to the sensing element. In all cases the duration of the run was such that

$$(c_1 + c_2)/c_0 < 0.01$$

and the contributions from the fictitious sources were neglected.

Computational Procedure and Results

The objective of the calculations was to determine the fluid-diffusion coefficient for each of the experimental runs. The experiment was designed such that the unsteady state diffusion equation, eq. (1), and the solution, eq. (2), were applicable. The calculated diffusion coefficient of dye was assumed to be identical to the fluid-diffusion coefficient, D_f.*

The data from a typical run as recorded on the strip chart are shown in Fig. 7 and as reduced to useful form are presented in Table 1.

The length of the dye injection was a measure of the finite time necessary for the dye injection to take place; one-half of this value

---

*The dye suspensions were slightly more dense than the water; hence, there could have been a gravity effect on the injected material. Measurements at different angles of tilt of the column would vary if a gravity effect was present. Runs 1 and 2 were made with the column tilted about 85° from the vertical; all other runs with the column vertical. The data indicate there was no detectable gravity effect.

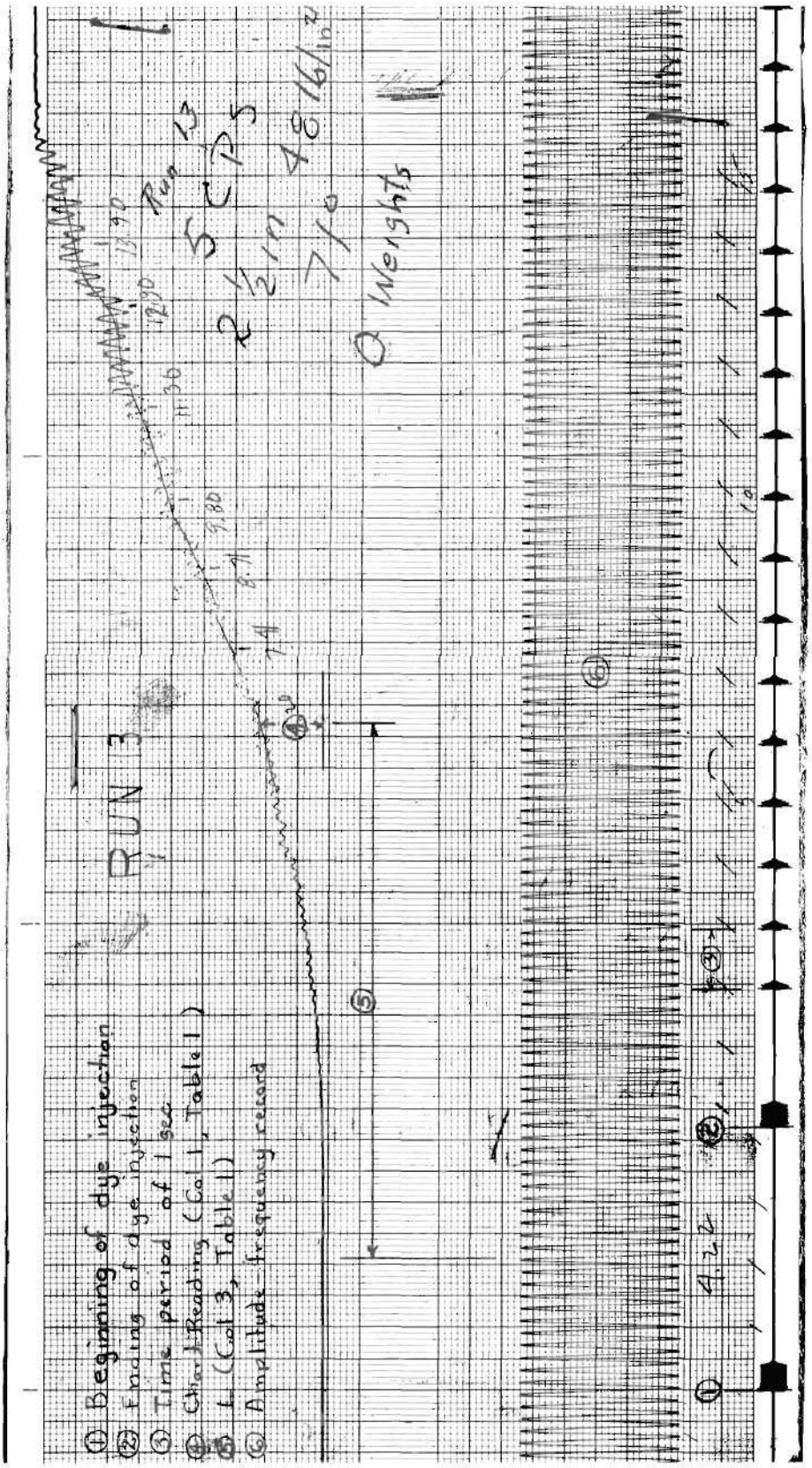

Figure 7. Typical Strip-Chart Record.

Table 1. Fluid Diffusion Data, Run 13

Column: Pressure, 10 psi; Length of dye injection, 4.22 cm
Pump: Amplitude, 2-1/2 in; Frequency, 5 cps; Pressure, 48 psi; Weights, 0; Spring, 16.

Chart Reading (cm)	Concentration, c (gm/l)	Length, L (cm)	100/L (cm^{-1})	ln C $\sqrt{L}$
1.0	0.225	8.6	11.61	-0.401
1.5	0.310	9.8	10.19	-0.0284
2.0	0.378	11.1	9.01	0.231
2.5	0.430	12.2	8.20	0.405
3.0	0.470	13.7	7.30	0.554
3.5	0.505	15.3	6.54	0.680
4.0	0.536	16.3	6.13	0.772

was added to the strip chart reading from the termination-of-injection mark to obtain the length referred to in Table 1.**

The following procedure was employed in order to evaluate D_f from the data using eq. (2)

$$c = \frac{K}{\sqrt{D_f t}} e^{-d^2/4 D_f t} \tag{2}$$

or

$$c\sqrt{t} = \frac{K}{\sqrt{D_f}} e^{-d^2/4 D_f t}$$

Taking the logarithm of both sides,

$$\ln c\sqrt{t} = -\frac{d^2}{4 D_f t} + \ln \frac{K}{\sqrt{D_f}} \tag{3}$$

For convenience of data reduction t is replaced with L/k in which k is the recorder-chart speed and L is the measured length on the strip chart. Inserting into eq. (3)

$$\ln c\sqrt{L} = -\frac{kd^2}{4 D_f L} + \ln \frac{K\sqrt{k}}{\sqrt{D_f}} \tag{4}$$

** Dye was injected at an approximately constant rate; however, the total amount of dye was varied from one and one-half to four cc with no apparent effect on the resulting diffusion coefficient determinations. This is interpreted as meaning that the method of averaging injection times is adequate.

If the values of ln $c\sqrt{L}$ are plotted as a function of 1/L, eq. (4) is a straight line with the slope, $- kd^2/4\ D_f$ (Fig. 8). The value of $kd^2/4\ D_f$ is 21.4 cm^{-1} for Run 13. Since d = 8.31 in or 21.1 cm and k = 0.99 cm/sec, the value of D_f is 5.16 cm^2/sec or $5.55(10^{-3})ft^2$/sec. A summary of all fluid-diffusion data is presented in Table 2. The complete data appear in Appendix III.

Analysis of Results

Significant progress has recently been made toward the goal of prediction of fluid-diffusion coefficients. The generalization can be simply stated as

$$D_f \propto E^{1/3} \mathcal{L}^{4/3} \tag{5}$$

in which E is the rate of energy dissipation per unit mass and $\mathcal{L}$ is a mean size of eddy. Many investigators have aided in the evolution of this principle, such as Richardson /13/, Kolmogoroff /14/, and Batchelor /15/. Orlob /16/ clearly stated this generalization and showed that eq. (5) was valid for lateral diffusion on the surface of two-dimensional open-channel flow. Orlob derived the expression

$$D_f = 0.0136\ E^{1/3} \mathcal{L}^{4/3} \tag{6}$$

from his experimental results. Taylor /17/ derived an expression for turbulent diffusion in a pipe

$$D_f = 0.052\ r u^* \tag{7}$$

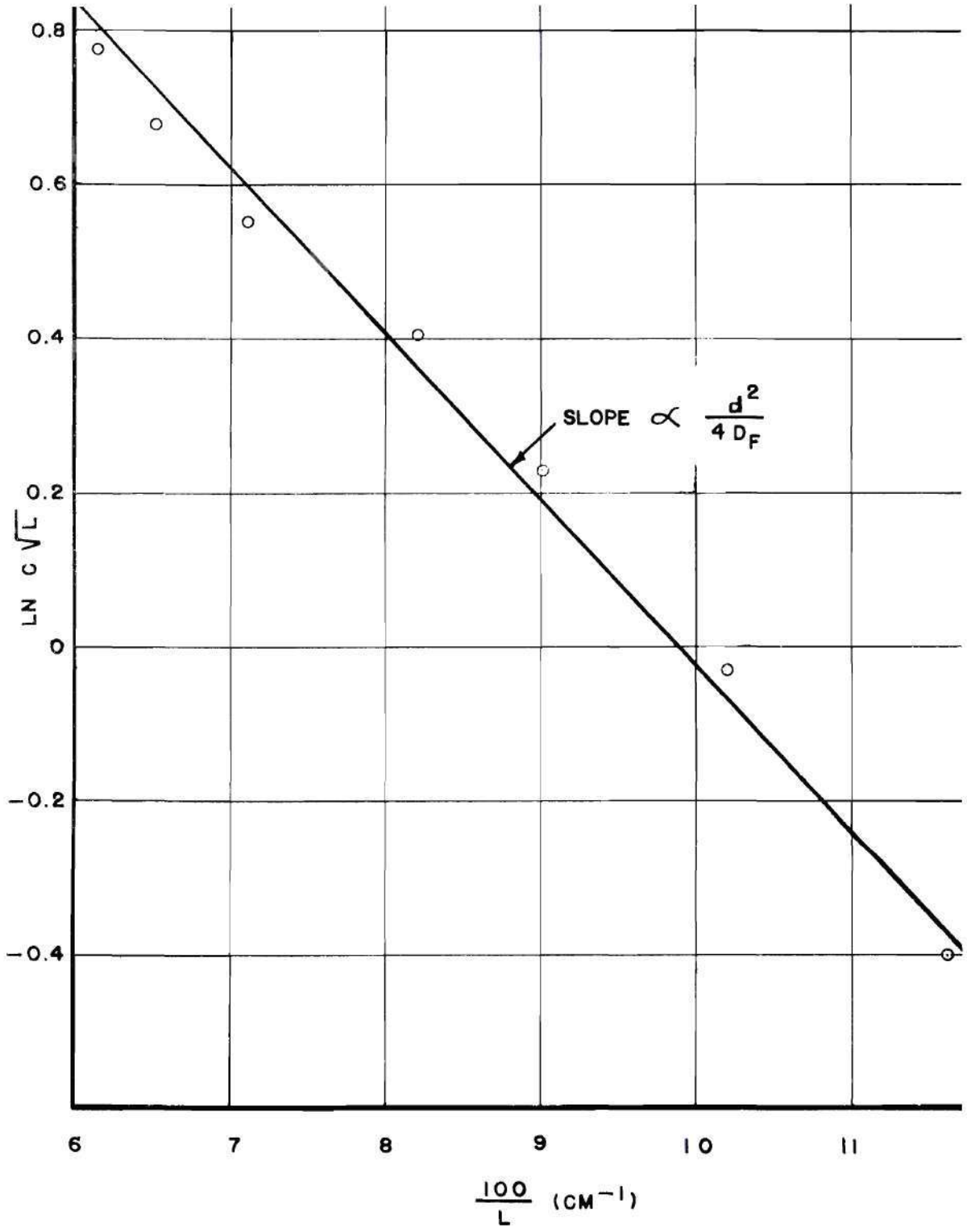

Figure 8. Fluid Diffusion, Run 13.

Table 2. Summary of Data - Eddy Diffusion of Fluid

Frequency f (cps)	Amplitude a_o (inches)	$(a_o f)$ (inches-cps)	Diffusion Coefficient D_f (square feet/second)
2	1.95	3.9	1.40×10^{-3}
	2.0	4.0	1.32
	2.5	5.0	1.72
	3.5	7.0	2.22
3	1.4	4.2	1.63
	1.5	4.5	1.89
	2.0	6.0	2.19
	2.5	7.5	2.81
	3.5	10.5	4.67
4	1.5	6.0	2.87
	1.6	6.4	2.36
	2.0	8.0	3.23
	2.4	9.6	3.40
	2.5	10.0	3.95
	3.5	14.0	5.84
5	0.95	4.95	2.12
	1.4	7.0	3.18
	2.0	10.0	4.18
	2.5	12.5	5.55
	2.85	14.25	7.25

In which r is the pipe radius and u* is the shear velocity. Eq. (7) can be rewritten as

$$D_f = 0.0413\left(\frac{u^*}{U}\right)^{1/3} E^{1/3} r^{4/3} = K_o E^{1/3} r^{4/3} \qquad (8)$$

in which U is the mean velocity. Values of K_o are presented in Table 3 as a function of Reynolds number in a smooth pipe. The values of K_o in Table 3 exhibit a modest change in a thousandfold change in the value of the Reynolds number. In addition, the coefficient K_o is approximately equal to the value 0.0136 obtained by Orlob. Since the values of K_o from the two determinations are in such good agreement, it seems reasonable to assume that the pipe radius is the mean eddy size. The radius intuitively appears too large for the mean size; hence, a more apt description of the characteristic eddy size may be the size of the largest eddies present in a significant number.

Table 3. Values of $0.0413(u^*/U)^{1/3}$ for a Smooth Pipe

Reynolds Number	U/u^*	$K_o = 0.0413(u^*/U)^{1/3}$
$3.72(10^3)$	14	0.0172
$3.86(10^4)$	19	0.0155
$3.74(10^5)$	24	0.0144
$3.55(10^6)$	29	0.0135

In order to relate the current experiments to the general law, eq. (5), values of the largest eddy size $\mathcal{L}$ and of the energy dissipation rate E will next be derived.

No direct measurement of mean eddy size was attempted but the fixed arrangement of pulsating jets and deflection wall insured that the eddy size $\mathcal{L}$ remained constant from run to run. When one nozzle was discharging into the chamber the four nearest neighbors were exhausting from the chamber. The nozzle arrangement is shown in Fig. 2. Since the adjacent nozzles were $\sqrt{2}$ in from center to center, the diameter of the largest eddy would be $2\sqrt{2}$ in. Therefore, in the subsequent analysis an $\mathcal{L}$ of 2.82 in was employed.

The rate of energy dissipation within the diffusion chamber can be evaluated by application of the work-energy equation to the fluid within a control volume which includes all the fluid within the chamber and cuts across the nozzles at the vena contracta of each exhausting nozzle as shown in Fig. 9. The fluid is assumed to have attained constant temperature.

$$-\rho \forall E + \int_{in} p\,u\,dA - \int_{out} p\,u\,dA = \frac{dE}{dt}$$

$$+ \int_{out} \left(\frac{\rho u^2}{2} + \gamma z\right) u\,dA - \int_{in} \left(\frac{\rho u^2}{2} + \gamma z\right) u\,dA \qquad (9)$$

in which

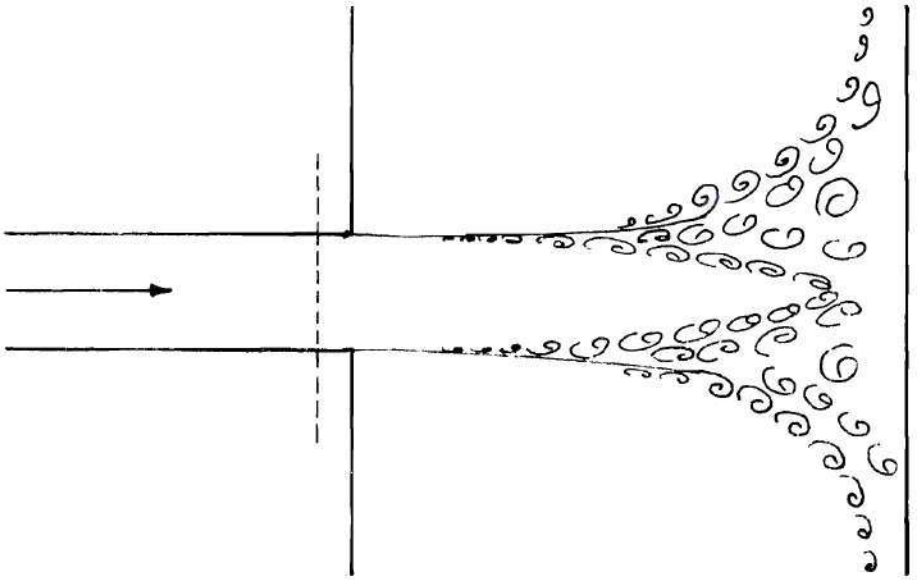

A) JETS DISCHARGING INTO CHAMBER

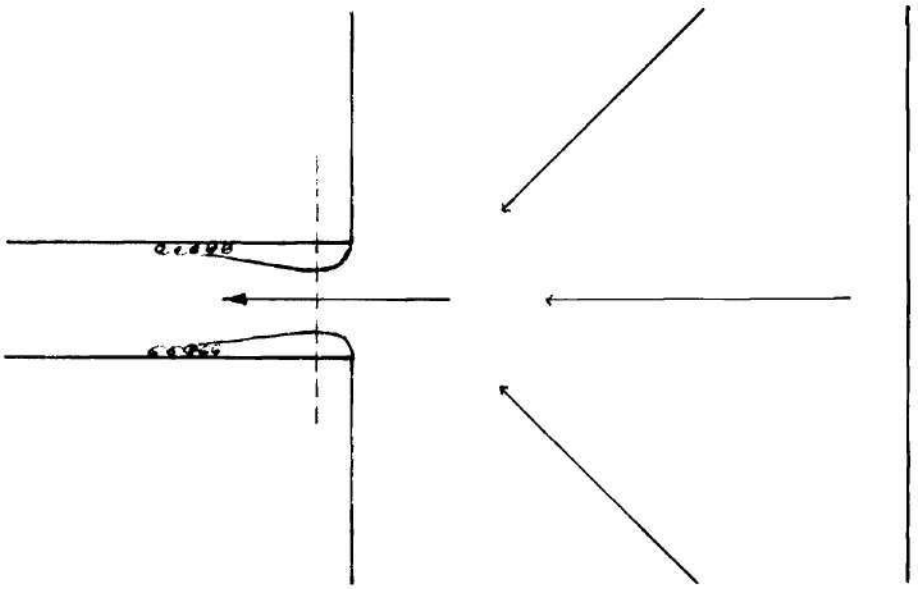

B) JETS DISCHARGING OUT OF CHAMBER

Figure 9. Flow Patterns from the Jets.

A = cross sectional area normal to the velocity,

E_o = energy of the matter within the control volume,

γ = specific weight,

p = pressure,

ρ = mass density,

u = velocity,

$\forall$ = total volume of diffusion chamber, and

z = elevation.

The last two terms on the RHS of eq. (9) are kinetic and potential energy flux terms. Since the potential energy of the fluid is unchanged in passing through the chamber, the terms $\gamma zudA$ can be omitted.

Since the velocity is zero over the control volume surface except at the nozzles the pressure-work integrals need only to be performed over the nozzle areas. In addition, the flow pattern from each discharging nozzle is similar to any other and the flow pattern into each exhausting nozzle is similar to any other. Thus, the integral of pressure work in can be performed over a single discharging nozzle and then simply multiplied by the number of discharging nozzles. A similar procedure is applicable for the evaluation of pressure work out at the exhausting nozzles.

Combining the pressure-work term with the energy-transport term at a discharging nozzle and taking the pressure within the chamber as being p_o, one obtains (Fig. 9a)

$$\int_{in\,(a\,nozzle)} \left(\frac{\rho u^2}{2} + p\right) u\,dA = \frac{\rho u^3}{2} A_n + p_o u A_n \qquad (10)$$

in which A_n is the cross sectional area of the nozzle.

The same operation can be performed at an exhausting nozzle. Two significant differences exist. First the pressure p_j at the control surface is less than p_o. Second the fluid separates from the sharp-edges nozzle forming a jet within the nozzle as shown in Fig. 9b. The area of the jet is $C_c A_n$ in which C_c is the coefficient of contraction. Assuming the flow is irrotational into the exhausting nozzle, the pressure p_j is

$$P_j = P_o - \frac{\rho u_j^2}{2} - \frac{\rho D_j}{\sqrt{8}} \frac{du_j}{dt} \tag{11}$$

in which D_j is the contracted-jet diameter. Therefore,

$$\int_{\text{out (a nozzle)}} \left(\frac{\rho u^2}{2} + p\right) u \, dA = P_o u_j A_j - \frac{\rho D_j}{\sqrt{8}} \frac{du_j}{dt} u_j A_j \tag{12}$$

Incorporating eq. (10) and eq. (12) into eq. (9)

$$-\rho \forall E = \frac{dE_o}{dt} + \frac{n}{2}\left(P_o - \frac{\rho D_j}{\sqrt{8}} \frac{du_j}{dt}\right) u_j A_j - \frac{n}{2}\left(P_o + \frac{\rho u^2}{2}\right) u A_n \tag{13}$$

in which n is the total number of nozzles in the diffusion chamber. Since $u_j A_j = u A_n$,

$$-\rho \forall E = \frac{dE_o}{dt} - \frac{n}{2} \frac{\rho D_j}{\sqrt{8}} \frac{du_j}{dt} u_j A_j - \frac{n}{2} \frac{\rho u^3}{2} A_n \tag{14}$$

Eq. (14) is applicable only when the velocity terms are positive. Consider the last term on the RHS. This term originated from discharging

nozzles and hence does not apply to exhausting nozzles. Similarly the second term on the RHS applies to exhausting nozzles and not to discharging nozzles.

In order to obtain an average energy dissipation rate in a complete cycle, it is necessary to integrate these last two terms over one-half cycle and to double the result since the same nozzles change roles in the second half of the cycle.

$$-\frac{\rho \forall}{T}\int_0^T E\,dt = \frac{1}{T}\int_0^T \frac{dE_0}{dt}\,dt$$

$$-\frac{\rho n}{T}\left\{\frac{D_j A_j}{\sqrt{8}}\int_0^{T/2} u_j \frac{du_j}{dt} + \frac{A_n}{2}\int_0^{T/2} u^3\,dt\right\} \qquad (15)$$

in which T is the period.

The first term on the RHS of eq. (15) represents the change of energy within the control volume during a cycle. Since the phenomenon is cyclic the energy states are equal at t = 0 and t = T. Hence, this term is zero in a cycle.

The water was forced through the nozzles by the piston pump. Since the fluid is incompressible, the nozzle velocities are related to the pump motion as follows. The pump displacement is

$$a = \frac{a_0}{2} \cos \frac{2\pi t}{T}$$

in which a_0 is the amplitude of the pump piston.

$$V_p = \frac{da}{dt} = \frac{\pi a_o}{T} \sin \frac{2\pi t}{T}$$

in which V_p is the velocity of the pump piston.

By continuity

$$V_p A_p = \frac{u A_p n}{2} = \frac{u_j A_j n}{2}$$

in which A_p is the pump-piston area. Therefore,

$$u = \frac{2\pi a_o A_p}{n A_n T} \sin \frac{2\pi t}{T} \tag{16}$$

and

$$u_j = \frac{2\pi a_o A_p}{n A_j T} \sin \frac{2\pi t}{T} \tag{17}$$

The term in eq. (15) containing du_j/dt will vanish upon evaluation of the integral.

Finally eq. (15) is simply

$$\rho \forall E = \frac{\rho n A_n}{2} \int_0^{T/2} u^3 \, dt$$

$$= \frac{4\pi^3 a_o^3 A_p^3 \rho}{n^2 A_n^2 T^4} \int_0^{T/2} \sin^3 \frac{2\pi t}{T} \, dt$$

$$= \frac{8\pi^2 A_p^3 \rho a_o^3 f^3}{3 n^2 A_n^2}$$

or

$$E = \frac{8\pi^2 A_p^3 (a_o f)^3}{3 n^2 A_n^2 \forall} \tag{18}$$

in which f is the frequency of the pump in cycles per sec. The numerical values of the quantities in eq. (18) are as follows:

$$A_p = 0.0197 \text{ ft}^2$$
$$n = 72$$
$$A_n = 0.000197 \text{ ft}^2$$
$$\forall = 0.0779 \text{ ft}^3$$

Combining the numerical values of $E^{1/3}$ and $\mathcal{L}^{4/3}$ into the generalized form of eq. (5)

$$D_f = 0.0282 K_o a_o f \tag{19}$$

in which the units of a_o are in and of f are cycles per sec.

The experimental results listed in Table 2 are graphically presented in Fig. 10 revealing (a) that the general diffusion law, eq. (5), is experimentally confirmed by these experiments and (b) that the coefficient of proportionality relating D_f and $E^{1/3}\mathcal{L}^{4/3}$ of 0.0136* is applicable to these results as well as Orlob's. In view of the great differences in manner of creating the diffusion mechanism, that is, in open-channel flow, in pipe flow, and with a pulsating-jet generator, the remarkable coincidence of results is indicative that the value of K_o is almost independent of the flow and geometric variables provided that the largest size of eddy is employed in evaluating $\mathcal{L}$. From the standpoint of engineering analysis this observation is extremely important since the value of energy dissipation rate E and largest eddy size can be estimated much more readily than D_f.

---

*From eq. (19), $D_f = K_o(0.0282)a_o f$, and from the equation shown in Fig. 10, $D_f = 3.9(10^{-4})a_o f$ it follows that $K_o = 0.0136$.

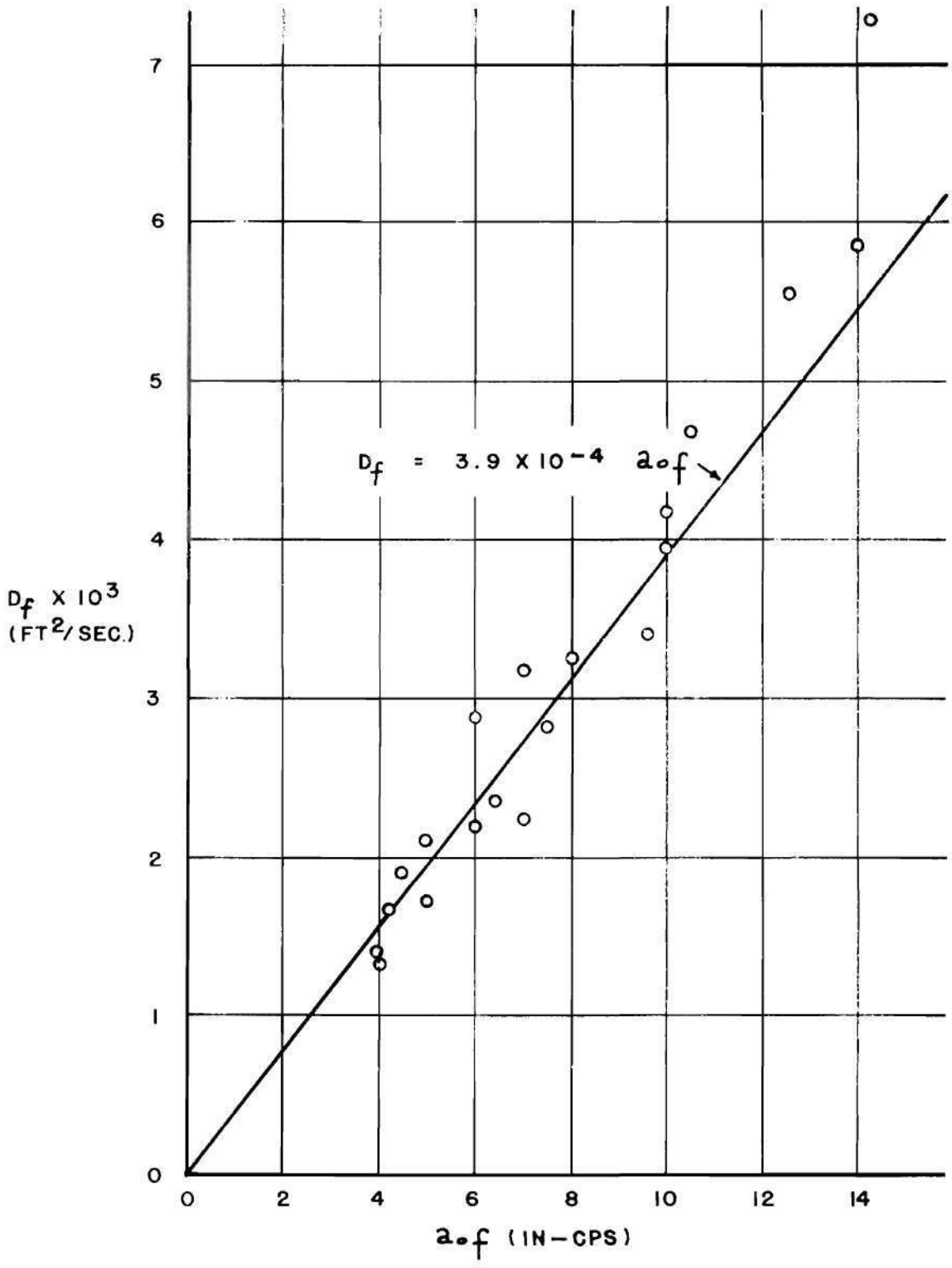

Figure 10. Relationship Between the Fluid-Diffusion Coefficient and the Product of Amplitude and Frequency.

CHAPTER III

EDDY DIFFUSION OF FOREIGN PARTICLES SUSPENDED IN A TURBULENT FIELD

The eddy diffusion of foreign particles, small solid spheres, was investigated experimentally. This investigation consisted of measuring the concentration distribution of solid particles suspended in a turbulent field.

The equilibrium steady state of the lateral transport of foreign particles in a turbulent field can be represesented by the diffusion equation,

$$F = - D_p \, dc/dz \tag{20}$$

in which D_p represents the eddy-diffusion coefficient, neglecting the molecular contribution. The molecular coefficients are approximately 10^{-8} /18/ compared to 10^{-3} for the observed eddy values. The steady state with respect to position is reached when the rate of transport in the positive z direction (vertical) is identical to the transport rate in the negative direction due to the particles settling under the force of gravity. The rate of transport F in the steady state is identical to the product of the settling velocity w and the point concentration c,

$$wc = - D_p \, dc/dz \tag{21}$$

If the coefficient of eddy diffusion and the settling velocity are

independent of position and concentration, eq. (21) may be integrated,

$$c/c^* = e^{-\frac{w(z-z^*)}{D_p}} \tag{22}$$

in which c* is the concentration at position z*. Concentrations of the solid particles were measured by tagging ion-exchange resin beads with radioactive cesium and measuring the count rate at various levels in the system. There was no net flow; hence, all of the beads remained in the system.

The choice of ion-exchange resins as particles simplified the particle description, because they were spherical in shape, constant in density, and uniform in size.

For sake of comparison, the turbulence field was the same as that used in the study of the fluid-particle diffusion. During the initial period of operation with the column oriented vertically, it was found that the concentration gradient of particles was too large. This large concentration gradient would have required that all significant measurements would have to be obtained near the bottom of the column where the background count was excessively large. The difficulty was overcome by tilting the column 77 degrees from the vertical. As shown later, in Analysis of Results, the tilting of the column did not alter the nature of the experiment other than to effect a scale reduction in the vertical coordinate, z.

Equipment

The eddy diffusion of solid particles was studied in a synthetic field of turbulence by observing radioactive ion-exchange resin beads.

The synthetic field of turbulence was the same as that used for the fluid-diffusion experiment except that two-tenths gram per gallon of MPX, a commercial non-ionic detergent, was added to the water to prevent beads from adhering to the walls of the system. Detergent in this quantity did not appreciably affect the physical properties of the fluid.

The angle of tilt of the brass side of the diffusion chamber, which was essential in describing bead transport, was measured with a vertical cathetometer manufactured by Gaertner Scientific Company.

The foreign particles were Dowex 50 X 16 ion-exchange resin beads, fifty to sixty mesh, in the H form. The H was replaced with a mixture of normal and radioactive cesium. These beads were co-polymers of styrene and divinyl benzene which contained nuclear sulfonic acid.

A scintillation crystal whose output was measured with a pulse height analyzer was used to observe the beads. This equipment is shown in Fig. 11. The crystal, Harshaw Type 7D4, was mounted in a probe, Type DP-3, which was attached to a traveling lead shield. The probe could be moved from one end to the other of the chamber on the side opposite to the pulsing jets. A slot 1/8 in by 2 in in the lead shield collimated the beam of radiation and limited it to one plane. The shield was counterbalanced to facilitate easy movement. The pulse height analyzer was the unit sold by Detectolab: consisting of a linear amplifier, Model DA5; of a single channel differential analyzer,

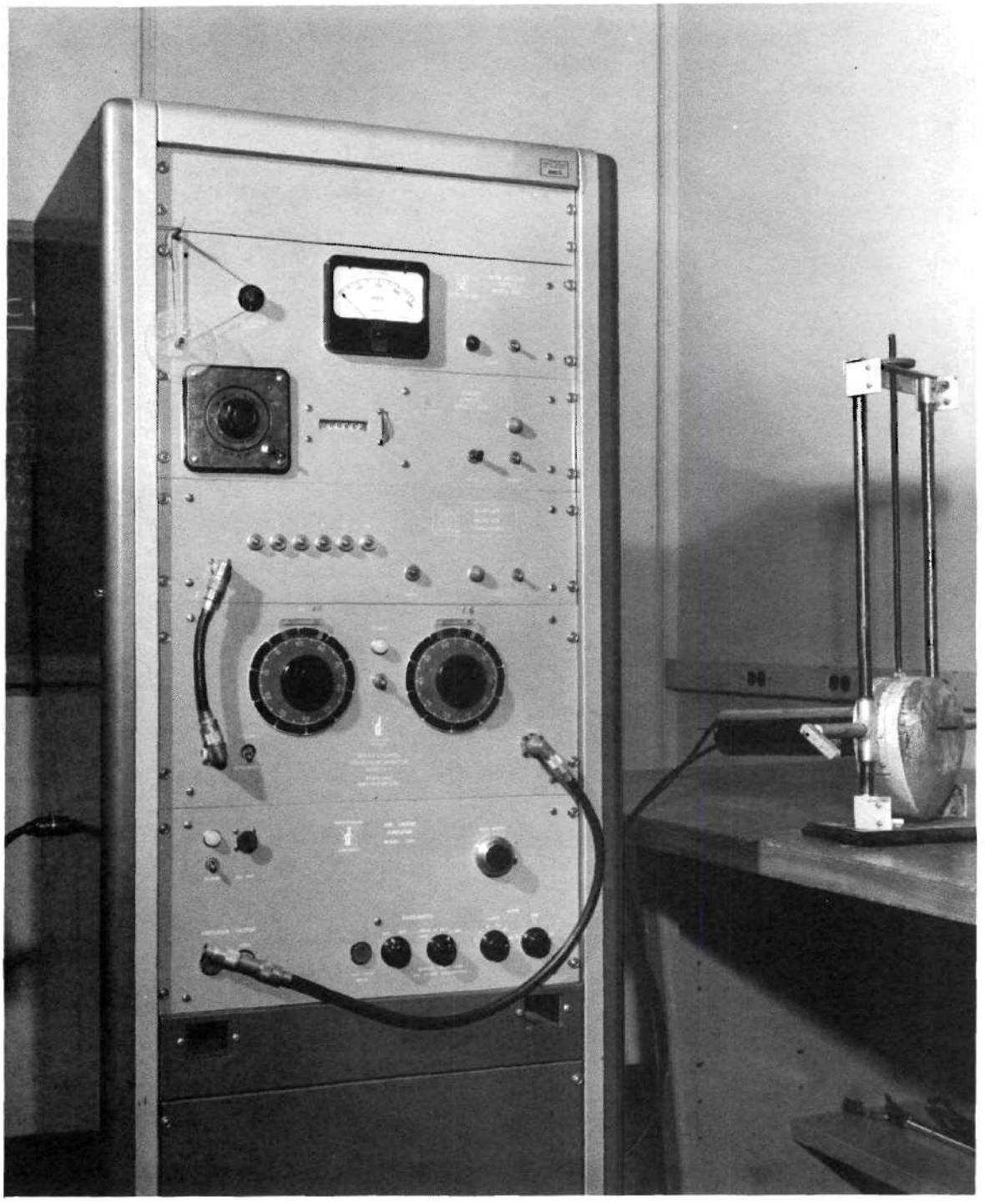

Figure 11. Radiation Sensing and Recording System.

Model DZ15; and of a scaler, Model DVI. A resistance type voltage divider and a Leeds and Northrup potentiometer, Model 8662, were used to check the stability of the high voltage supply.

Experimental Procedure

The turbulence generator operation was identical to that used in the fluid-diffusion determinations.

The ion-exchange resin beads were separated by wet screening within a range of fifty to sixty mesh. The beads were then washed with six-normal hydrochloric acid until the efflux was no longer green, then washed with distilled water. Radioactive cesium chloride solution was contacted with the beads for eight hours so that an equilibrium would be reached. The strength of the cesium chloride solution was such that the beads exhibited a count-rate of about one count per minute per bead, from a position as close to the scintillation crystal as possible (the thickness of a glass beaker). After contact with the radioactive solution the beads were washed with distilled water and stored under water. Photomicrographs and fall velocity determinations were made on a portion of these beads. Bead diameters were measured and sphericity verified directly from the photomicrographs, and densities were calculated from the fall-velocity data. Fall velocities were made by timing the fall of one hundred individual beads (Appendix IV).

Data to describe the motion of the beads were taken with the diffusion chamber tilted so that a few beads were in the top portion of the chamber even at low frequencies and small amplitudes. This angle was not changed but was checked from run to run. A traverse consisted of

the determination of count-rate over the height of the chamber of background or of beads. Enough beads were used to cover the bottom of the diffusion chamber to a depth of one-quarter inch with no fluid motion.

Operating conditions for the pulse height analyzer were varied until cesium radiation was readily measurable; however, no attempt was made to optimize these conditions. The conditions used were high voltage, 1100 volts; gain, 8; bandwidth, 0.5 mc; and bandwidth of the energy spectrum, 10 units. Before each run the energy level of maximum count rate was determined and used for the measurement; this level was about 24 on the scale. A timer in the scaler control unit determined the length of time that counts were compiled. This timer was set for a long enough time so that a minimum of 10,000 counts was accumulated in order to provide a statistical accuracy of one per cent in the measurement. Count rates were measured at various heights in the chamber. Then a lead block was inserted into the slit of the collimator. Background measurements were made with a second traverse and with the turbulence generator running in the same manner.

Measurement of the position of the probe and of the angle of tilt of the chamber were accomplished by use of a cathetometer. Two dots were placed on the side of the chamber in the same vertical line. A measurement of the vertical distance between points and their distance apart, 56.56 centimeters, was sufficient to define the angle of tilt of the chamber.

Computational Procedure and Results

The objective of the calculations was to determine the particle-diffusion coefficient, D_p, for each of the experimental runs. The experiment was designed such that the steady-state diffusion, eq. (21), and the solution, eq. (22), were applicable.

The data from runs U and W are presented in Table 4 in order to demonstrate the method of computation of results. Fig. 12 is a graphical presentation of the count-rate as a function of elevation. Since the collimator slit was completely blocked with a lead filler in Run W, the count rate for this run is background count. In order to determine the count rate attributable to radioactive particles in front of the collimator slit, the background count was subtracted from the data of Run U. Actually smoothed curves were passed through the data points as shown in Fig. 12 with the differences between the two curves being determined from the graphs at selected intervals of $z-z^*$.

The following procedure was employed in order to evaluate D_p from the data using eq. (22). Taking the logarithm of both sides of eq. (22) and rearranging,

$$\ln c = -\frac{w(z-z^*)}{D_p} + \ln c^* \qquad (23)$$

Since the count rate, C, was proportional to the concentration, c, C may be substituted for c in eq. (23),

$$\ln C = -\frac{w(z-z^*)}{D_p} + \ln C^* \qquad (24)$$

Table 4. Particle-Diffusion Data. Runs U and W.

Column	U	W	Counter	U W	Pump	U	W
Top	43.615	43.655	High Voltage	1100	Amplitude	$3\frac{1}{2}$"	
Bottom	30.655	30.680	Gain	8 x 1	Frequency	2 cps	
Pressure	9	9	Bandwidth	0.5 mc	Pressure	35 psi	$32\frac{1}{4}$ psi
z*	17.30	17.32		10	Springs	8	8
					Weights	All	All
					Temp.	78°	74°

z (cm)	c	R	z - z*	C (counts/min)	Remarks
19.540	24	186-7/6	2.24	1985	U
20.660	24	176-11/9	3.36	1253	
21.960	24	180-16/14	4.66	824	(without
23.220	24	176-47/18	5.92	628	lead in
24.495	24	183-63/22	7.20	535	slit)
25.645	24	76-29/10	8.35	489	
20.060	24	146-38/6m 17s	2.76	1493	
19.540	24.5	190-58/10	2.22	1222	W
20.700	24	194-19/14	3.38	888	
21.985	24	182-5/17	4.67	685	(with lead
23.350	24	165-31/19	6.03	557	in slit)
24.710	24	155-13/20	7.39	497	
21.280	24	173-16/19	3.96	792	
20.060	24.5	166-57/10	2.74	1068	

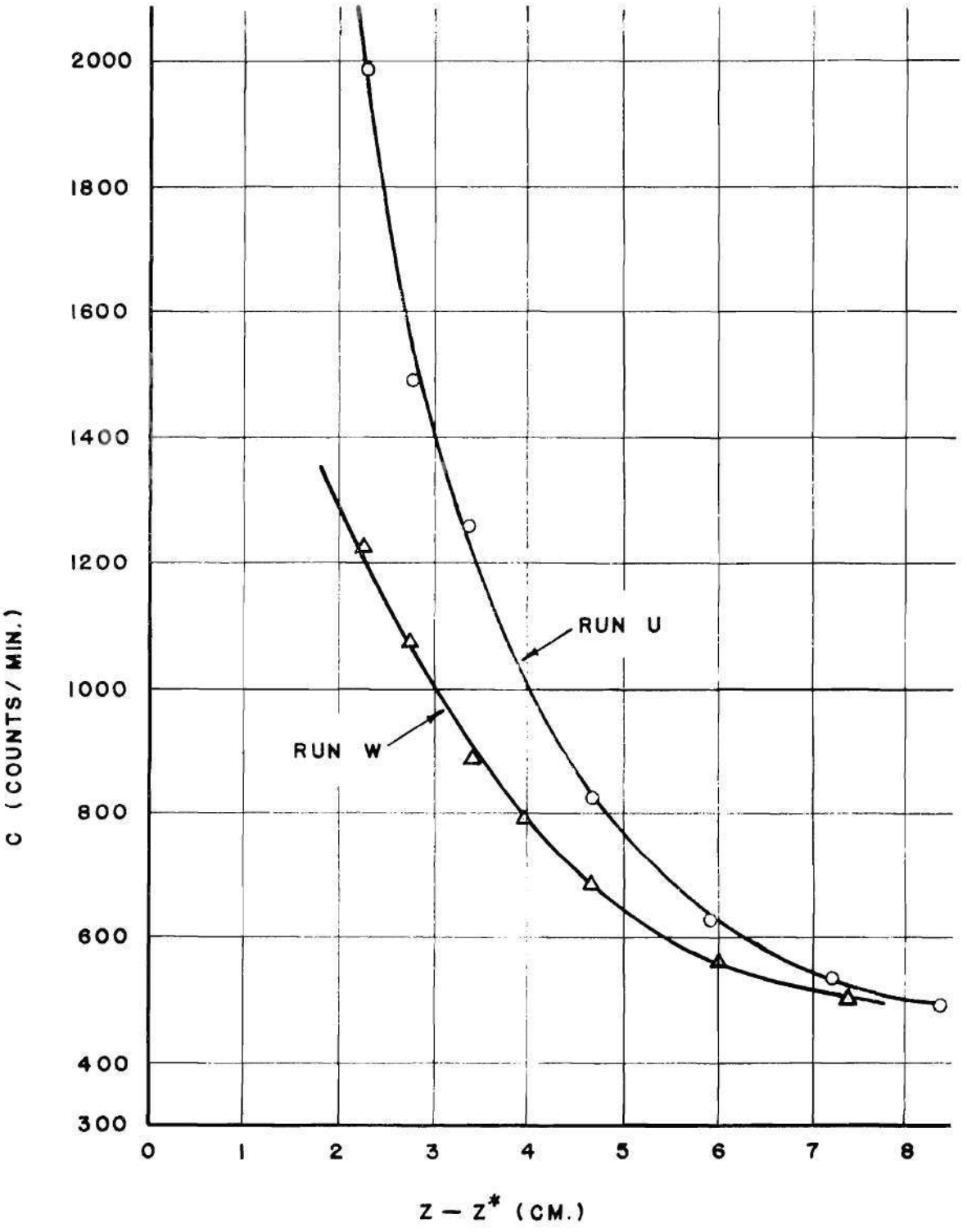

Figure 12. Raw Data from Runs U and W.

If the values of ln C in which $C = C_u - C_w$ are plotted as a function of $(z-z^*)$, eq. (24) is a straight line with the slope, $-w/D_p$ (Fig. 13). The value of $-w/D_p$ for Runs U and W is $-0.667\ cm^{-1}$. Since $w = 3.85 \times 10^{-2}$ ft/sec at 76°, the value of D_p is $1.894 \times 10^{-3}\ ft^2/sec$.

A summary of all particle-diffusion data is presented in Table 5. The complete data appear in Appendix V.

Analysis of Results

Using the same logic as for the fluid-diffusion results, the particle-diffusion coefficient D_p is presented in Fig. 14 as a function of $a_o f$. Again the general diffusion law, eq. (5), is a reasonable representation of the experimental results. A direct comparison of D_p and D_f (Figs. 10 and 14) at identical values of $a_o f$ is valid since the same turbulence generator was used in both sets of experiments. The outstanding observation is that the particle-diffusion coefficient D_p is appreciably less than the corresponding value of D_f. In fact, D_p is approximately $0.67\ D_f$. In the following, possible causes for the large difference between D_p and D_f will be investigated.

Experimental Deviations from Idealized Model.--In spite of the attempt to perform the experiments with an ideal diffusion chamber and sensing method, approximations were necessary. Several conditions in which the experiment deviated from the mathematical model will be discussed in order to evaluate the effect of these approximations upon the experimental results, Table 5.

The total differential equation, eq. (21), which was integrated to obtain the solution, eq. (22), is a one-dimensional equation with

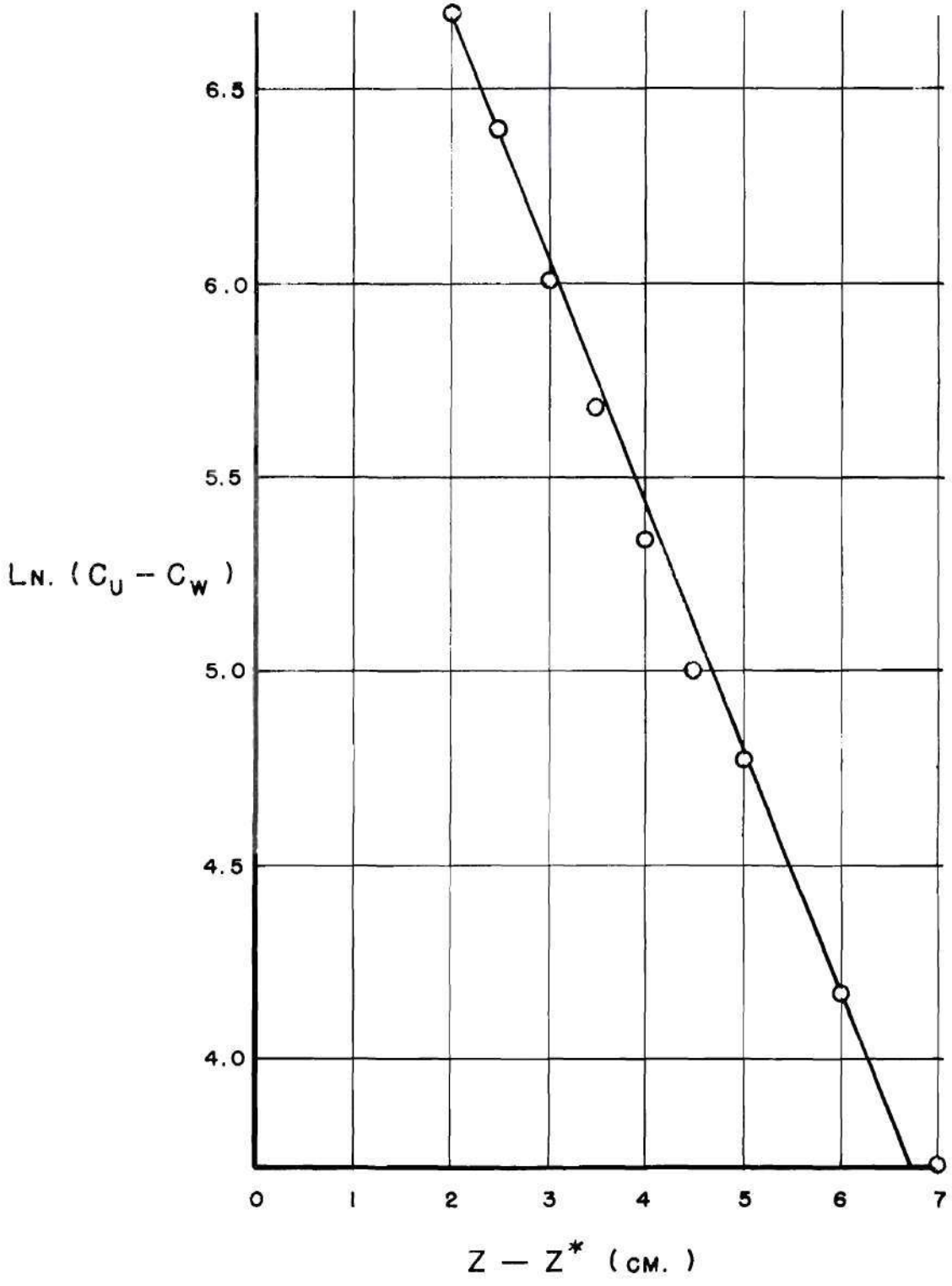

Figure 13. Reduced Data from Runs U and W.

Table 5. Summary of Data - Eddy Diffusion of Beads

Frequency f	Amplitude a_o	$a_o f$	Diffusion Coefficient x 10^3 D_p x 10^3
(cps)	(in.)	(in.-cps)	(ft^2/sec)
2	2.0	4.0	0.94
2	2.5	5.0	1.25
2	3.5	7.0	1.89
3	1.5	4.5	1.13
3	2.0	6.0	1.52
3	2.5	7.5	1.64
3	3.5	10.5	3.72
4	1.5	6.0	1.44
4	2.0	8.0	1.99
4	2.5	10.0	3.37
4	3.5	14.0	3.68
5	1.5	7.5	2.15
5	2.0	10.0	2.92
5	2.5	12.5	4.57
5	3.0	15.0	4.30

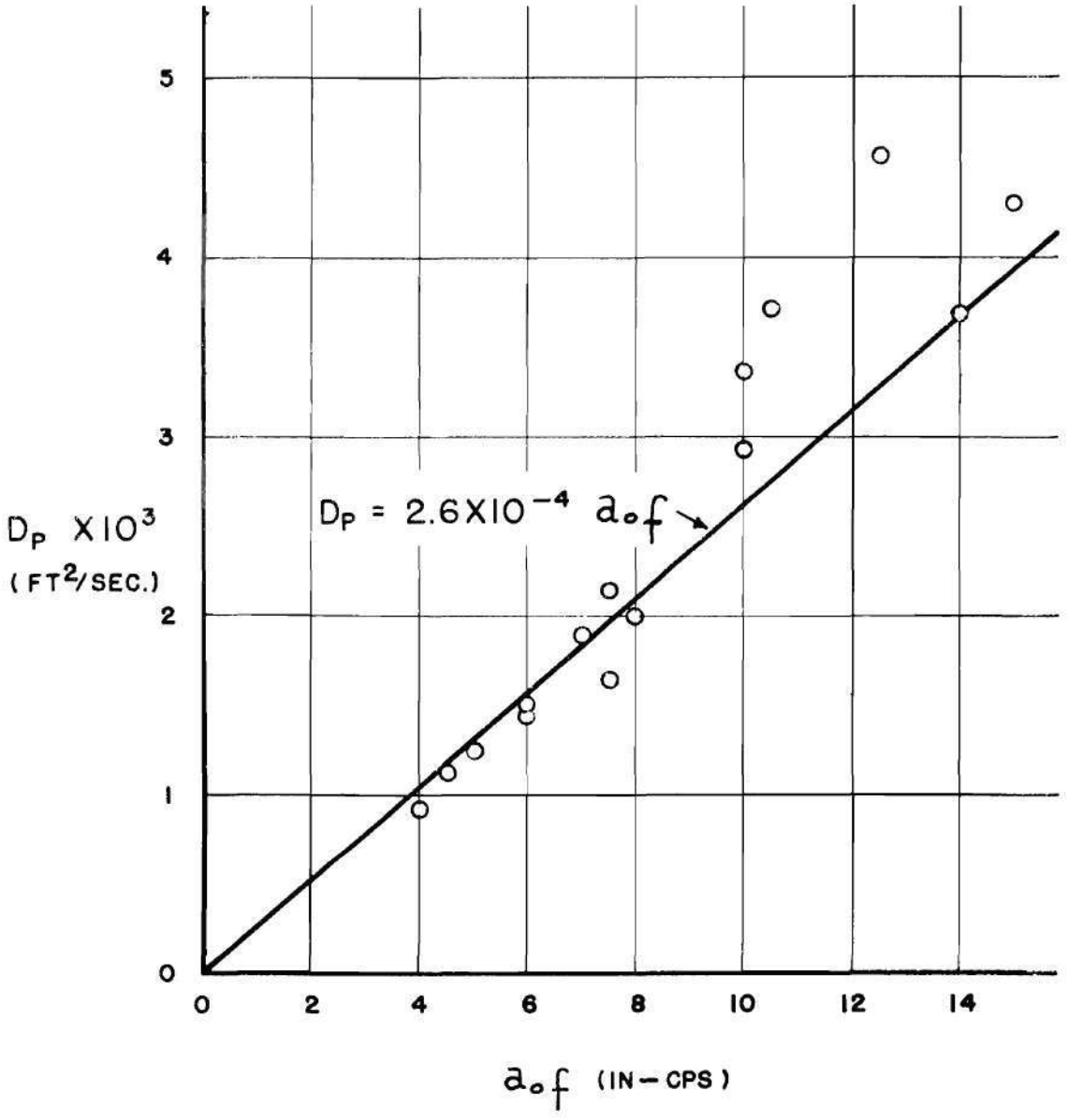

Figure 14. Relationship Between the Particle Diffusion Coefficient and the Product of Amplitude and Frequency.

the concentration being constant on a horizontal plane. The concentration determination was made in a plane perpendicular to the column axis. When the column is tilted, the plane of concentration determination is no longer horizontal but is inclined as shown in Fig. 15. Substituting

$$z - z^* = z_o - z^* + y\cos\alpha$$

into eq. (22)

$$c = c^* e^{-\frac{w}{D_p}(z_o - z^* + y\cos\alpha)} \tag{25}$$

The sensing device obtains a count of the particles in the plane perpendicular to the face and extending from y = 0 to y = y_1, that is

$$C \propto \int_0^{y_1} c\, dy \tag{26}$$

Substituting eq. (25) into eq. (26) and integrating

$$C \propto c^* e^{-\frac{w}{D_p}(z_o - z^*)} \left\{\frac{D_p}{y_1 \cos\alpha}\right\}\left\{1 - e^{-\frac{w}{D_p} y_1 \cos\alpha}\right\} \tag{27}$$

Since y_1, α, and w are constants throughout the column and D_p can be considered to be constant on the average, eq. (27) can be written in

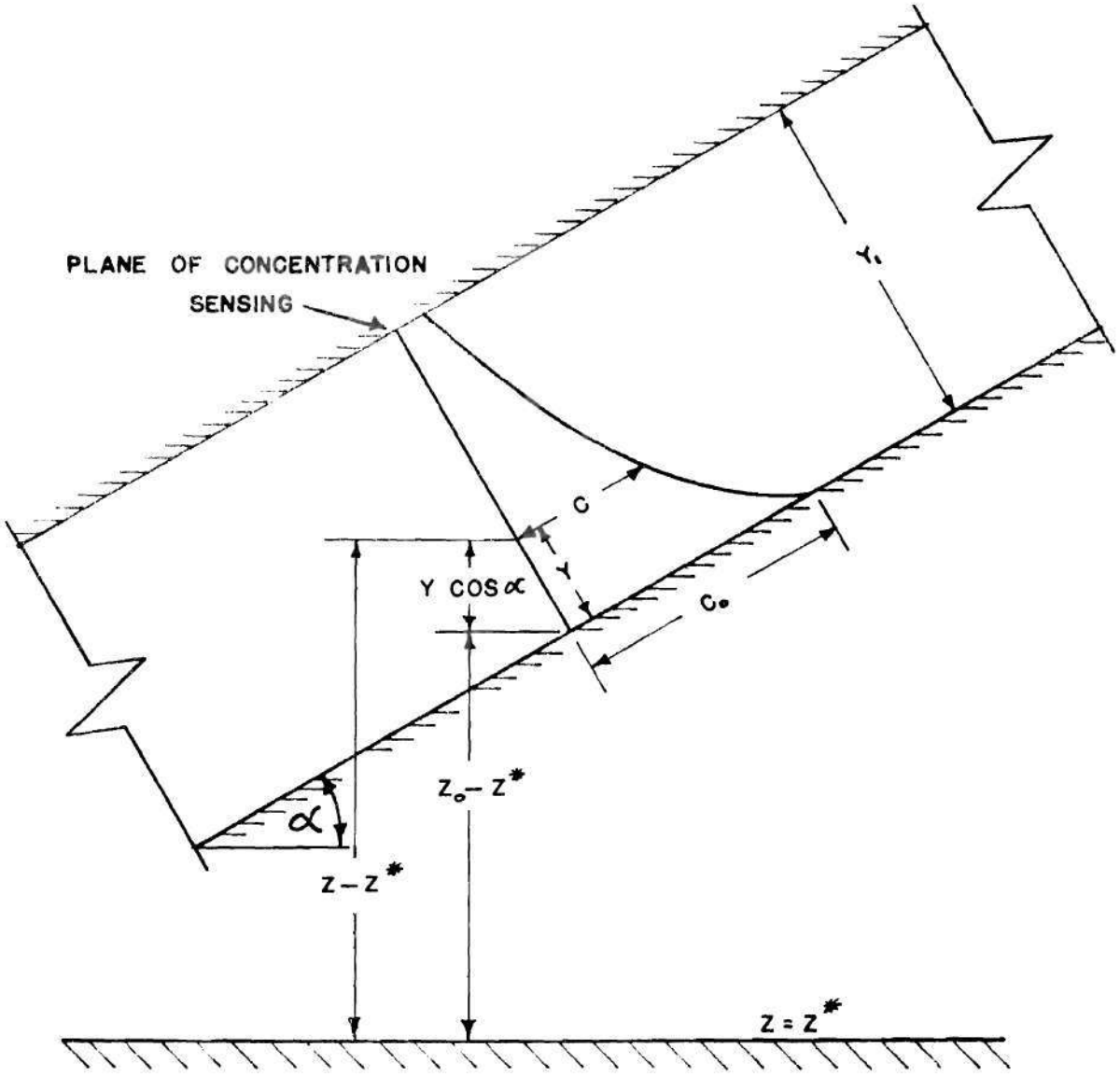

Figure 15. Plane of Concentration Sensing Not Horizontal.

ratio form as follows

$$C/C^* = e^{-\frac{w}{D_p}(z_o - z^*)}$$

which is exactly the equation, eq. (22), employed in the reduction of the data.

When the column was tilted, an appreciable portion of the particles rolled along the plastic face of the column rather than being moved in suspension. Eagleson and Dean /19/ have investigated motion under similar conditions, that is, oscillatory rolling motion of a spherical particle on a smooth plane. A conclusion of their work is that the drag force of the fluid on rolling particles is about tenfold that on suspended particles provided that all other conditions are identical. This information applied to the equation of motion is indicative that rolling particles will more closely follow their fluid neighbors than suspended particles. Consequently, this effect would result in the values of D_p being larger for the rolling and suspended particles than for all particles in suspension.

The sensing element departed from the ideal in that particle counts were obtained throughout a volume region in front of the detector rather than on a plane. In order to evaluate the significance of this departure from the ideal the relative count rate between the region adjacent to the near wall and the far wall will be evaluated. In Fig. 16 are shown cross sections through the collimator and column. Particles emit radiation in all directions but the detector senses only that

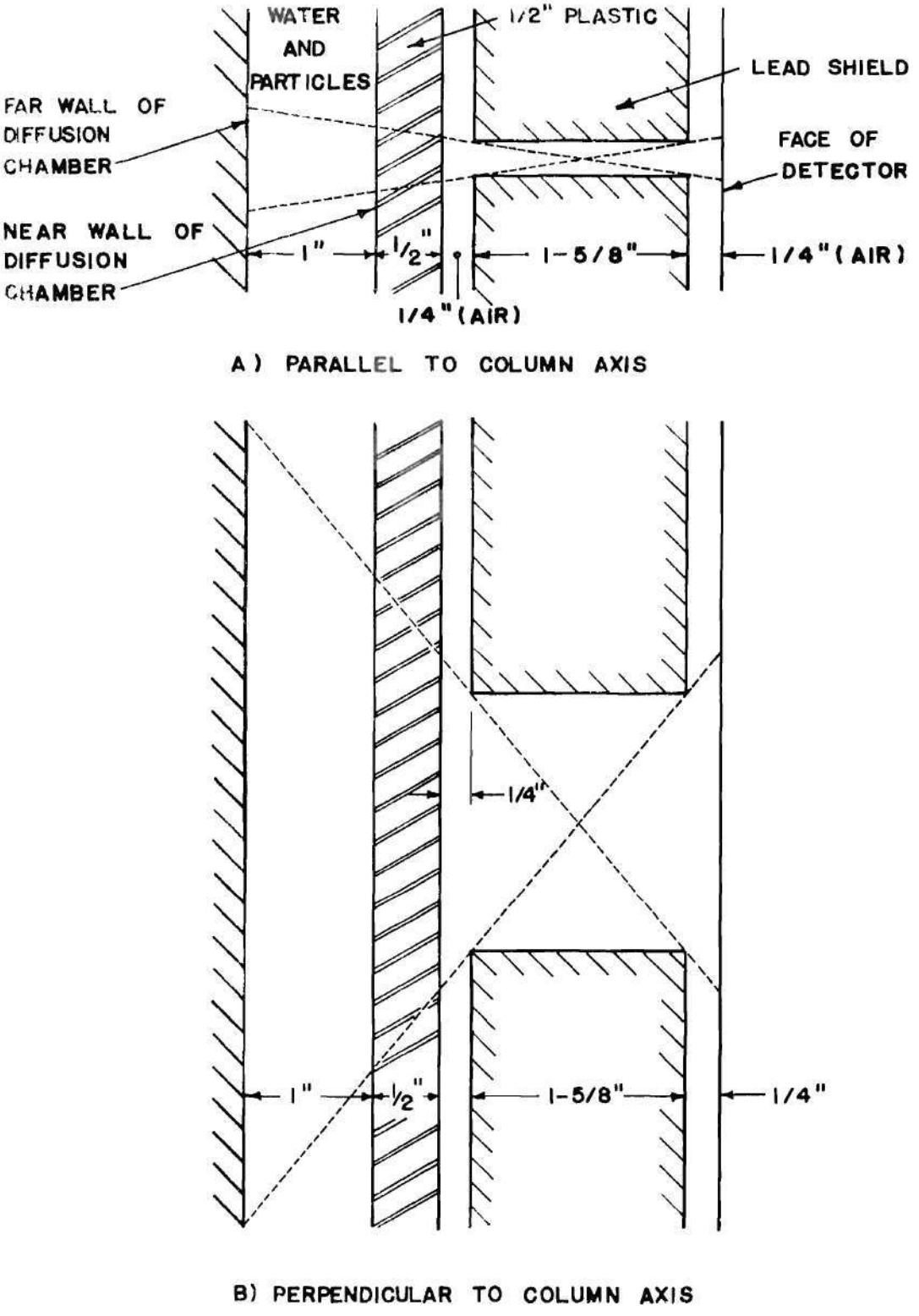

Figure 16. Cross Sections Through Collimator.

emission which travels directly to the face of the detector. For purposes of analysis, the volume region from which emission is received is considered as a central region and a fringe region.

The central region is the volume which is directly in front of the collimator slit. Considering the solid angle subtended, only 0.196 per cent of the total emission is detected of particles adjacent to the far wall. Similarly 0.375 per cent is detected of particles adjacent to the near wall. The energy radiated from the particles adjacent to the far wall must pass through an inch of water in addition to the path traveled by the radiation from particles adjacent to the near wall. The scattering and adsorption of energy is given by the exponential law for which the adsorption coefficient is 0.085 cm^{-1} for cesium 137 emission in water /20/. Assuming a uniform concentration of particles, the detected emission from the central region of the far wall and that of the central region of the near wall is

$$I_{fc} \approx k_1 (0.00196)(1/8 \text{ in} \times 2 \text{ in})(0.806) = 0.000395\, k_1$$

$$I_{nc} \approx k_1 (0.00375)(1/8 \text{ in} \times 2 \text{ in}) = 0.000938\, k_1$$

in which k_1 includes the effect of adsorption and scattering through the plastic and air and also includes the scintillation counter efficiency.

The fringe region is the volume surrounding the central region in which the solid-angle subtended is less than that of the central region. Beyond, the outer edge of the fringe region, no emission reaches the counter. In fact the solid-angle subtended decreases from the value in

the central region to zero at the outer edge. Also the path along which energy can be adsorbed and scattered is longer in the fringe region than in the central region. A mean path length was used to evaluate the loss in the fringe region. Combining all of these factors the detected emission of the fringe region from the far wall is

$$I_{fF} \approx k_1 (0.00196/2)(2.12\ in^2)(0.786) = 0.00163\ k_1$$

and from the near wall is

$$I_{nF} \approx k_1 (0.00375/2)(0.667\ in^2) = 0.00127\ k_1$$

Combining the two regions the ratio

$$I_f / I_n = 0.92$$

In other words, if the particle concentration were uniform, the counter would register slightly more counts from the particle closer to the near wall. In fact a collimator could be designed for which the detection efficiency was constant regardless of particle position from the counter. However, since the concentration ratio $C_{y=y_1}/C_{y=0}$, from eq. (25) is constant across the column at any station of measurement no error is introduced since ratios of mean count rate are utilized.

The above development is more significant from the standpoint of demonstrating that a finite volume is observed rather than the plane as visualized in the mathematical model. The width of the truncated pyramid

of observation was 0.395 in on the far wall and 0.240 in on the near wall. The mathematical model is formulated in terms of elevation or vertical direction only. The inclination of the column thus tends to reduce the above values to approximately 0.090 in and 0.055 in in the vertical, respectively. While these dimensions are finite, no appreciable error is introduced by considering the observation to be planar.

The next topic to be discussed is that of the effect of the sediment traps behind the column opposite to the scintillation counter. Fig. 17 is a sketch through the axis of the column. The count rate at observation station 1 is the sum of the count from the column plus that from the sediment traps. At station 1

$$C_1(\text{column}) = K C_0 e^{-(w/D_p)(b/2)}$$

$$C_1(\text{trap}) = K_1 C_0 e^{-(w/D_t)(b/2)}$$

$$C_1(\text{total}) = C_0 \left\{ K e^{-(w/D_p)(b/2)} + K_1 e^{-(w/D_t)(b/2)} \right\}$$

At station 2

$$C_2(\text{column}) = K C_0 e^{-(w/D_p)(3b/2)}$$

$$C_2(\text{trap}) = K_1 C_0 e^{-(w/D_p)b} \left\{ e^{-(w/D_t)(b/2)} \right\}$$

$$C_2(\text{total}) = C_0 e^{-(w/D_p)b} \left\{ K e^{-(w/D_p)(b/2)} + K_1 e^{-(w/D_t)(b/2)} \right\}$$

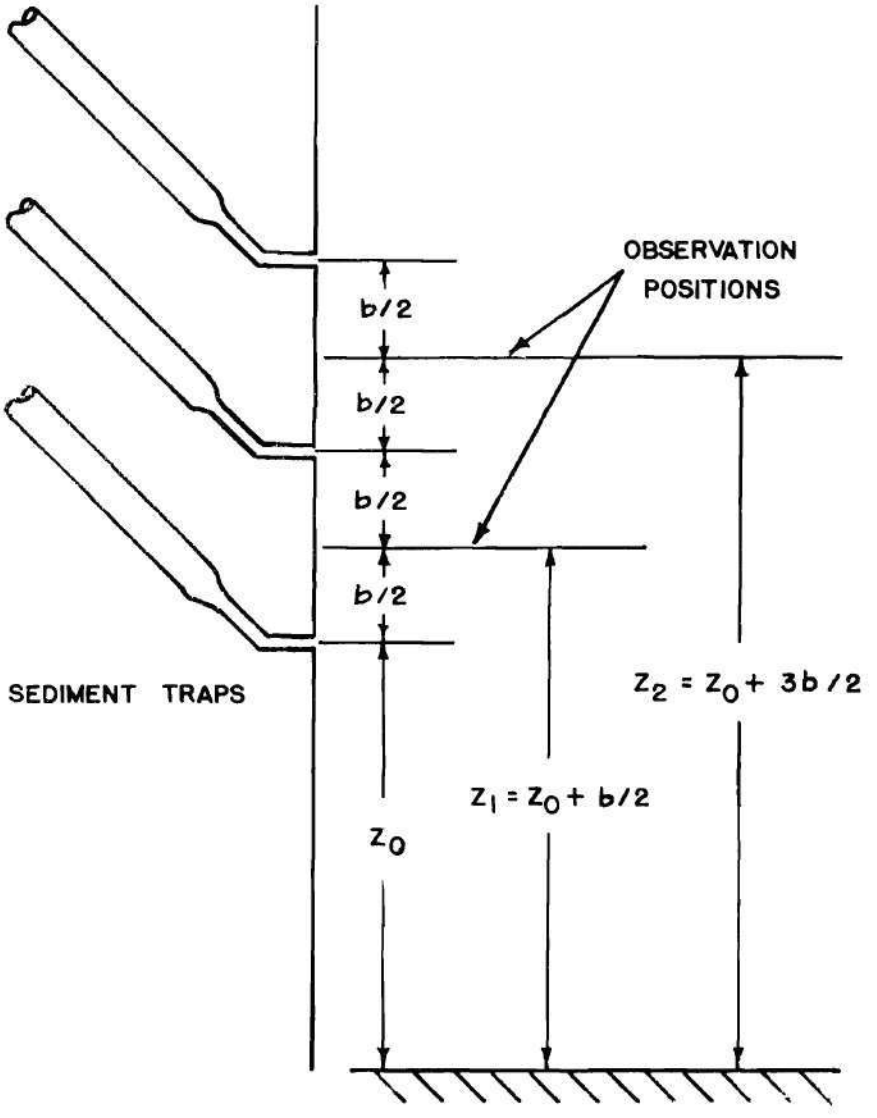

Figure 17. Effect of Sediment Traps upon Count Rate.

in which D_t is the diffusion coefficient in the sediment traps. Therefore

$$C_2 / C_1 = e^{-(w/D_p)b}$$

This result is a demonstration that the sediment trap emission has no effect on the count-rate ratio if the observation stations are taken at homologous points between the lines of jets or at intervals of b. Since the value of K_1 is about 5 per cent of that of K no detectable cyclic deviation from the model function, eq. (24), is anticipated nor could any cyclic deviation be detected from the experimental results, for example, in Fig. 13. The conclusion is that sediment-trap emission has no influence in the determination of D_p.

A possible explanation for the low experimentally determined values of D_p in comparison to those of D_f is that D_f is a variable across the column. With the column titled, the majority of the particles both in rolling motion and in suspension were in the vicinity of the plastic wall opposite to the wall containing the pulsing jets. For this explanation to be rational, D_f would have to be greater near the pulsing-jet wall and decrease toward the plastic wall. However, if a spatial variation exists one would expect the larger values of D_f to exist near the plastic wall since the penetrating jet is deflected by the plastic wall. Thus the larger eddies should form near the plastic wall.

Theoretical Explanations for $D_p < D_f$.--The solid particles being more dense than the fluid could be expected to be out of phase and to oscillate

with a lesser amplitude than the neighboring fluid particles. Hence, this inertial effect might be the explanation for the values of D_p being less than values of D_f. An estimation of this effect can be obtained by consideration of the motion of a single spherical particle in a moving fluid. The general equation of motion has been presented by Tchen /5/ and was integrated for the case of simple harmonic fluid motion in which the drag force was proportional to the difference between the fluid and the particle velocity. Using this solution, with the ion-exchange resin beads of this study, the particle amplitude is found to be 0.987 or larger of the fluid amplitude. Such a small difference in amplitudes is entirely insufficient to explain the large differences of D_p and D_f found in this study. In order to insure that the inertial effect is truly negligible, the writer numerically integrated the equation of motion for a spherical particle having properties equivalent to the mean value of the sampled particles and for simple-harmonic fluid motion having a maximum velocity equal to the maximum estimated within the column. The solution was performed with the fluid-drag force being proportional to the square of the difference between the fluid and the particle velocity and with a steady-state drag coefficient. Again the amplitude difference was negligible.

All of the previous discussion has been confined to the particle-diffusion coefficient; however, in the reduction of the data by means of eq. (24) as illustrated in Fig. 13, the experimentally determined values were of w/D_p. The tacit assumption was made that the settling velocity w is identical in an eddy-diffusive flow situation as in a still fluid. The equation of motion for a single particle in a turbulent field and

and with the buoyant weight included has been presented by Tchen /5/. However, the equation has not been solved except for grossly simplified cases. Professor Carstens* has shown that for simple harmonic fluid motion with a drag force proportional to the relative velocity, the settling velocity should decrease. At the University of Iowa studies are currently in progress to experimentally determine the settling velocity of particles in a fluid which is oscillated harmonically. Also the Iowa Researchers, Dr. Brush and Mr. Ho, are performing numerical solutions in which non-linear resistance terms are included. Their work /21/ also indicates that w tends to decrease with frequency and amplitude of the fluid oscillation. However, for the density and size of the particles used in this study the decrease would be negligible.

The above discussion of settling velocity pertained to particles in suspension; but with the inclined diffusion chamber some of the particles were in contact with the wall. The settling velocity of these particles would be less than the suspended particles because of the increased resistance force resulting from the proximity of the wall and from the physical restraint of the wall. From the data presented by Eagleson /19/, the settling velocity of the particles rolling down the wall would be about 1/24 that of the suspended particles. An experimental determination of the proportion of rolling particles to suspended particles was not possible. Nevertheless, the mean value of w would be somewhat less if the rolling particles were correctly evaluated.

---

*This information was communicated to the writer in a discussion.

A significant paper has recently been published by Torobin and Gauvin /22/ in which a dramatic decrease in the particle drag coefficient was experienced when the intensity of turbulence was large. Such a decrease in C_d would result in a corresponding increase of settling velocity w. Torobin and Gauvin measured the particle motion of a single spherical particle in a wind tunnel. Their explanation of the large decrease in the value of C_d in comparison to that of a particle falling in a still fluid was that the boundary layer around the particle became turbulent. Their explanation was based upon the observation that the critical Reynolds number for transition was a function of the ratio of the intensity of turbulence to the mean relative velocity and that the observed decrease was similar to that observed with stationary spheres at much greater values of the particle Reynolds number. This study is indicative that the boundary layer around a free rather than a fixed particle becomes turbulent at a much lower value of the Reynolds number.

The existence of turbulent boundary layers around the free particles is a plausible explanation of the difference between the calculated values of D_p and the experimentally determined values of D_f. However, difficulty is experienced in attempting to apply Torobin's and Gauvin's results because an unknown percentage of the particles was in contact with the sloping plastic face of the diffusion column. The fall velocity of a particle in suspension is

$$w = K^*/\sqrt{C_d}$$

The fall velocity of a particle restrained by the sloping face of the column is

$$w_r = K^* (\sin\alpha)^{3/2} / \sqrt{C_d}$$

Further, it is assumed that the C_d's are the same for the suspended particles as for the restrained particles and that a decimal portion N of the total particles is restrained. Thus a mean fall velocity of the aggregrate is

$$\bar{w} = \frac{K^*(1-N) + K^* N (\sin\alpha)^{3/2}}{\sqrt{C_d}}$$

Since the still-fluid settling velocity w_s is equal to $K^* / \sqrt{C_{ds}}$, the ratio $\bar{w}/w_s$ is

$$\frac{\bar{w}}{w_s} = \sqrt{\frac{C_{ds}}{C_d}} \left\{ 1 - N + N (\sin\alpha)^{3/2} \right\} \qquad (28)$$

Before proceeding further, it is necessary to estimate a reasonable value of D_p/D_f. The method of analysis is similar to that presented by Carstens /23/ in which the equation of motion for a single spherical particle in an oscillating fluid was integrated and the value of D_p/D_f was equated to $(x_o/\ell_o)^2$ in which x_o and ℓ_o are the particle and fluid amplitudes, respectively. The essential difference is that

in the present analysis the drag force on the particle is represented by the law of turbulent drag rather than that of viscous drag. The equation of motion of a particle in an oscillating fluid without gravity is

$$M_o\ddot{x} = M\ddot{\ell} + k_m M(\ddot{\ell} - \ddot{x}) + \frac{C_d \rho A^* |\dot{\ell} - \dot{x}|(\dot{\ell} - \dot{x})}{2} \qquad (29)$$

in which

M_o = particle mass,

M = displaced-fluid mass,

C_d = coefficient of drag,

A^* = projected area of particle,

k_m = virtual-mass coefficient,

ρ = mass density,

$\ddot{x}$, $\dot{x}$, x = particle acceleration, velocity, and displacement, and

$\ddot{\ell}$, $\dot{\ell}$, ℓ = fluid acceleration, velocity, and displacement.

The various forces on the spherical particle are the fluid pressure-gradient force $M\ddot{\ell}$, the virtual-mass effective force $k_m M(\ddot{\ell}-\ddot{x})$, and the drag force $\rho \frac{C_d A^*}{2} |\dot{\ell} - \dot{x}|(\dot{\ell} - \dot{x})$.

Unfortunately, eq. (29) is nonlinear. The equation can be linearzied by means of an equivalent viscous-damping coefficient C_v.

$$C_v = \frac{\rho C_d A^* |\dot{\ell} - \dot{x}|}{2} \qquad (30)$$

The solution of eq. (29) with a viscous-damping coefficient is

$$x = x_o \sin(\omega t + \phi) \tag{31}$$

in which the phase angle ϕ is defined by

$$\tan\phi = \frac{(C_v/M\omega)(1-\rho_s/\rho)}{(C_v/M\omega)^2 + (\rho_s/\rho + k_m)(1+k_m)} \tag{32}$$

and the maximum particle amplitude is defined by

$$\left(\frac{x_o}{l_o}\right)^2 = \frac{(C_v/M\omega)^2 + (1+k_m)^2}{(C_v/M\omega)^2 + (\rho_s/\rho + k_m)^2} \tag{33}$$

The equivalent viscous-damping coefficient C_v is formulated by equating the energy dissipation of the turbulent-drag force to the energy dissipation of an equivalent viscous-drag force in a harmonic cycle.

$$\int_0^T (C_v u_r)\, u_r\, dt = \int_0^T \left(\rho \frac{C_d A^*}{2} |u_r|\, u_r\right) u_r\, dt \tag{34}$$

in which u_r is the relative velocity between the fluid and the particle.

$$u_r = u_{rm} \cos \omega t \tag{35}$$

Substituting eq. (35) into eq. (34), performing the integration, and solving for the equivalent viscous-damping coefficient

$$C_v = \frac{8}{3\pi} \frac{C_d \rho A^*}{2} |u_{rm}| = \frac{8}{3\pi} \frac{C_d \rho A^*}{2} |\dot{\ell} - \dot{x}|_{max} \tag{36}$$

In order to solve for the maximum relative velocity, eq. (30) is substituted into eq. (29) and the equation is rearranged as follows

$$(M_o + k_m M) \frac{du_r}{dt} + C_v u_r = (M_o - M) \frac{d^2 \ell}{dt^2} \tag{37}$$

in which the fluid motion is prescribed as

$$\ell = \ell_o \sin \omega t \tag{38}$$

Substituting eq. (38) into eq. (37), integrating, and solving for u_{rm}

$$u_{rm} = \frac{(\rho_s/\rho - 1) \ell_o \omega}{\sqrt{(C_v / M\omega)^2 + (\rho_s/\rho + k_m)^2}} \tag{39}$$

Finally eq. (36) is substituted into eq. (39) and the combined equation is solved for the maximum relative velocity u_{rm}

$$u_{rm} = \frac{\pi d \omega}{2\sqrt{2}\, C_d} \left\{ \sqrt{\left(\frac{\rho_s}{\rho} + k_m\right)^4 + \frac{16}{\pi} C_d^2 \left(\frac{\ell_o}{d}\right)^2 \left(\frac{\rho_s}{\rho} - 1\right)^2} - \left(\frac{\rho_s}{\rho} + k_m\right)^2 \right\}^{1/2} \tag{40}$$

Reasonable values of D_p/D_f or $(x_o/\ell_o)^2$ can be calculated by substituting the appropriate values into eqs. (40), (36), and (33), successively. The value of C_d of 0.2 is employed assuming completely turbulent boundary layer around all particles. The value of k_m is taken as one half as for irrotational flow around a sphere. The value of ρ_s/ρ was 1.31. A mean value for ℓ_o of the fluid motion was calculated based on the continuity of flow between adjacent rows of jets. The value of the particle mean diameter was 0.0117 in. The resulting values of ℓ_o/d are 1.28, 1.71, 2.14, 2.56, and 2.99 for pump amplitudes of 1.5, 2.0, 2.5, 3.0, and 3.5 in, respectively.

$$D_p/D_f = 0.69 \tag{41}$$

with an insignificant variation with pump amplitude.

With the value of $D_p = 0.69\, D_f$ the ratio of the actual mean settling velocity $\bar{w}$ to the still-fluid settling velocity w_s can be obtained.

$$\frac{\overline{w}}{0.69\,D_f} = \frac{w_s}{2.6\,(10^{-4})\,a_o f}$$

in which the value $2.6(10^{-4})a_o f$ was determined earlier as shown in Fig. 14. Hence,

$$\frac{\overline{w}}{w_s} = \frac{(0.69)(3.9)(10^{-4})\,a_o f}{2.6\,(10^{-4})\,a_o f} \approx 1 \qquad (42)$$

A brief review is in order to evaluate the fortuitous result expressed in eq. (42). In the analysis of results leading to the results shown in Fig. 14, the still-fluid settling velocity w_s was employed. The particles falling in a still fluid were surrounded by laminar flow. If the hypothesis that the boundary layer became fully turbulent around the particles in the column, the fall velocity would be greatly increased except for the sloping wall of the column which restrained the fall. The conclusion is simply that the increase of fall velocity by change in flow regime and the decrease by virtue of wall restraint counterbalanced each other with the result that values of D_p presented on Fig. 14 are valid without correction of the fall velocity.

In order for the result expressed in eq. (42) to have occurred an appreciable percentage of the particles experienced wall restraint. Equating eqs. (28) and (42) and using $C_{ds} = 9.04$, $C_d = 0.2$, and $\alpha = 13$ degrees, the value of N is found to be 0.95. In other words, a given

particle on the average experienced wall restraint 95 per cent of the time and was in true suspension 5 per cent of the time.

The only other explanation offered for the observed results is that diffusion by eddies of the same magnitude or smaller than the size of the particles is significant. In other words the possibility exists that small eddies could diffuse fluid but be too small to diffuse particles. However, the possibility of appreciable diffusion being attributable to eddies of 0.012-in diameter in a field where the largest eddy is 2.82 in in diameter is inconceivable.

CHAPTER IV

CONCLUSIONS AND RECOMMENDATIONS

The following conclusions were drawn from this study.

(1) The most important finding was that the general diffusion equation, as derived by Orlob from Kolmogoroff's work, namely,

$$D \propto E^{1/3} \ell^{4/3}$$

was substantiated by fluid and particle diffusion measurements in a unique turbulent field.

(2) The constant of proportionality in the general diffusion equation was shown to be approximately the same for homogeneously turbulent fluid diffusion in open-channel flow, pipe flow, and flow within the diffusion chamber of this study.

(3) For the particles and system employed, the particle diffusion coefficients, defined in terms of the particle fall velocities in a still fluid, were 33 per cent less than the corresponding fluid coefficients.

(4) Early transition to turbulence in the boundary layer surrounding a particle, as reported by Torobin and Gauvin, is the most probable reason for the reduction in diffusion coefficients. A detailed discussion of the manner in which this transition affects the particle diffusion was presented.

(5) The turbulence generator is a useful device in studies involving turbulent transport. The principal virtue of this device

is that energy dissipation rate E is controllable and determinable while the eddy size $\mathcal{L}$ remains constant. Other advantages are that the diffusion chamber contains no mechanical agitators and that there is no net flow through the system.

The following recommendations are made to guide any future work in this field.

(1) A series of experiments should be performed to define completely the mean eddy size in terms of the system geometry. Since the turbulence generator used in this study provided a turbulent field in which the energy dissipation was independent of the eddy size, this type generator should be used in these experiments.

(2) The diffusion chamber should either be positioned vertically or horizontally for any additional particle-diffusion experiments, in order that all secondary effects are eliminated.

(3) The dependence of the particle-diffusion coefficient on particle density and size should be determined experimentally. The results of Torobin and Gauvin should be utilized in planning and interpreting these experiments.

APPENDICES

APPENDIX I

ELECTRONIC SYSTEMS

This appendix contains the wiring diagrams of the three electrical systems which were not commercial instruments. They are shown in Figs. 18, 19, and 20.

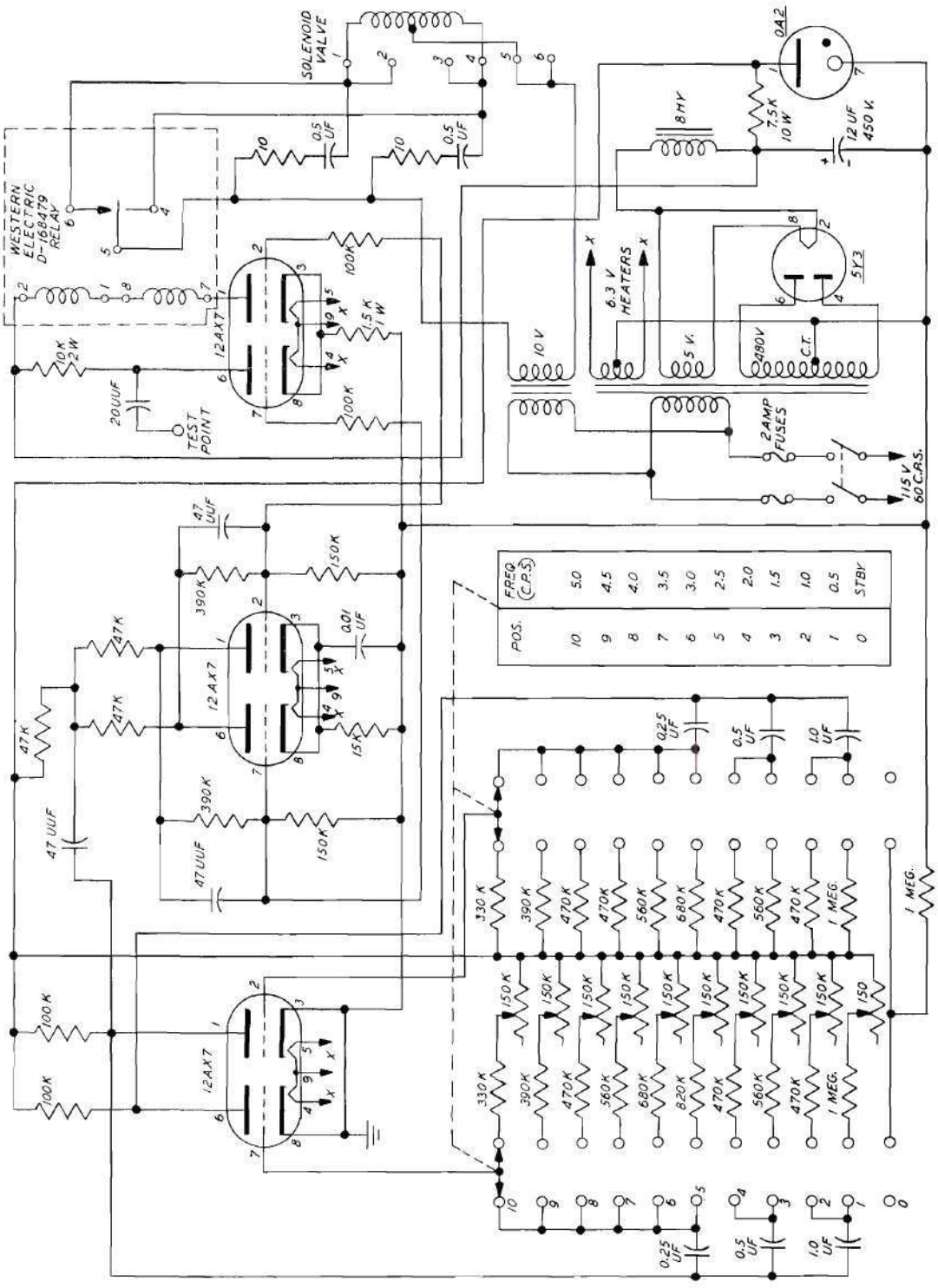

Figure 18. Wiring Diagram of Timer.

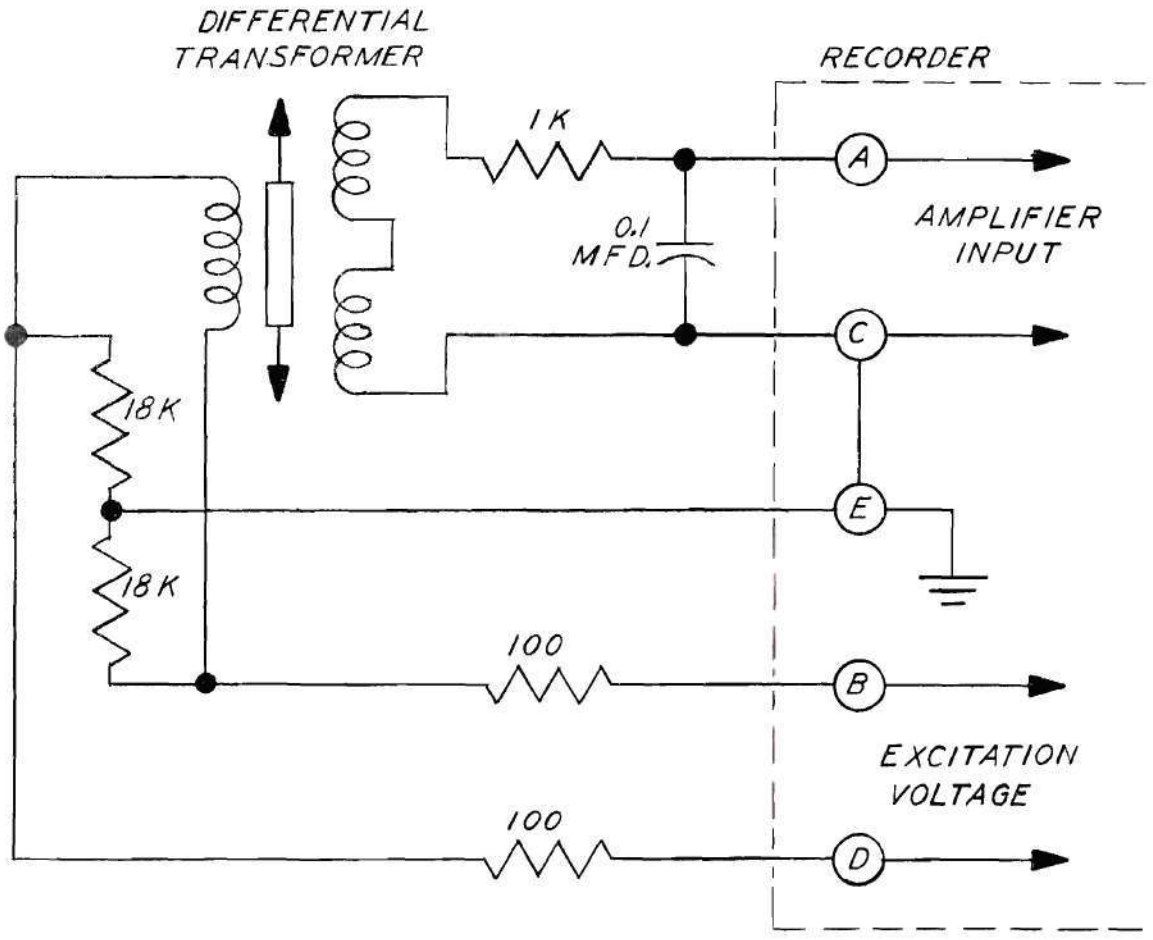

Figure 19. Differential-Transformer Circuit.

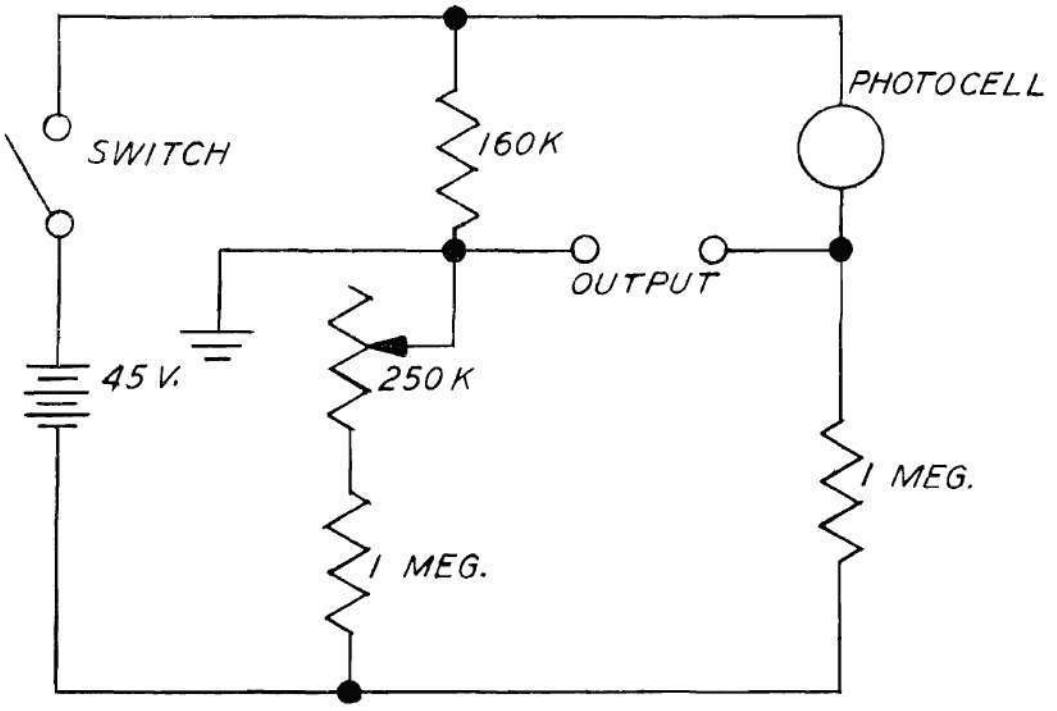

Figure 20. Photocell Balancing Circuit.

APPENDIX II

PHOTOCELL CALIBRATION

This section contains data of the calibration of the photocell used in the investigation.

Table 7 and Fig. 21 pertain to the calibration of the photospectrometer; Table 8 and Fig. 22, the calibration of the photocell.

Table 6. Photospectrometer Calibration

Weight of Black Dye of Specific Gravity = 1.0 (grams)	Diluting Water (ml)	Concentration (gm/l)	% Transmittance
0.0711	475	0.150	87.5
0.1075	333	0.322	79
0.1804	303	0.595	64
0.3623	330	1.097	45
0.5408	330	1.641	29.5

Table 7. Photocell Calibration

% Transmittance	Chart Reading (mm)	Concentration Dye (gm/l)
83.4	11	0.245
74.2	23	0.404
67.0	37	0.518
74.2	22	0.404
81.8	15	0.270
67.0	37	0.518

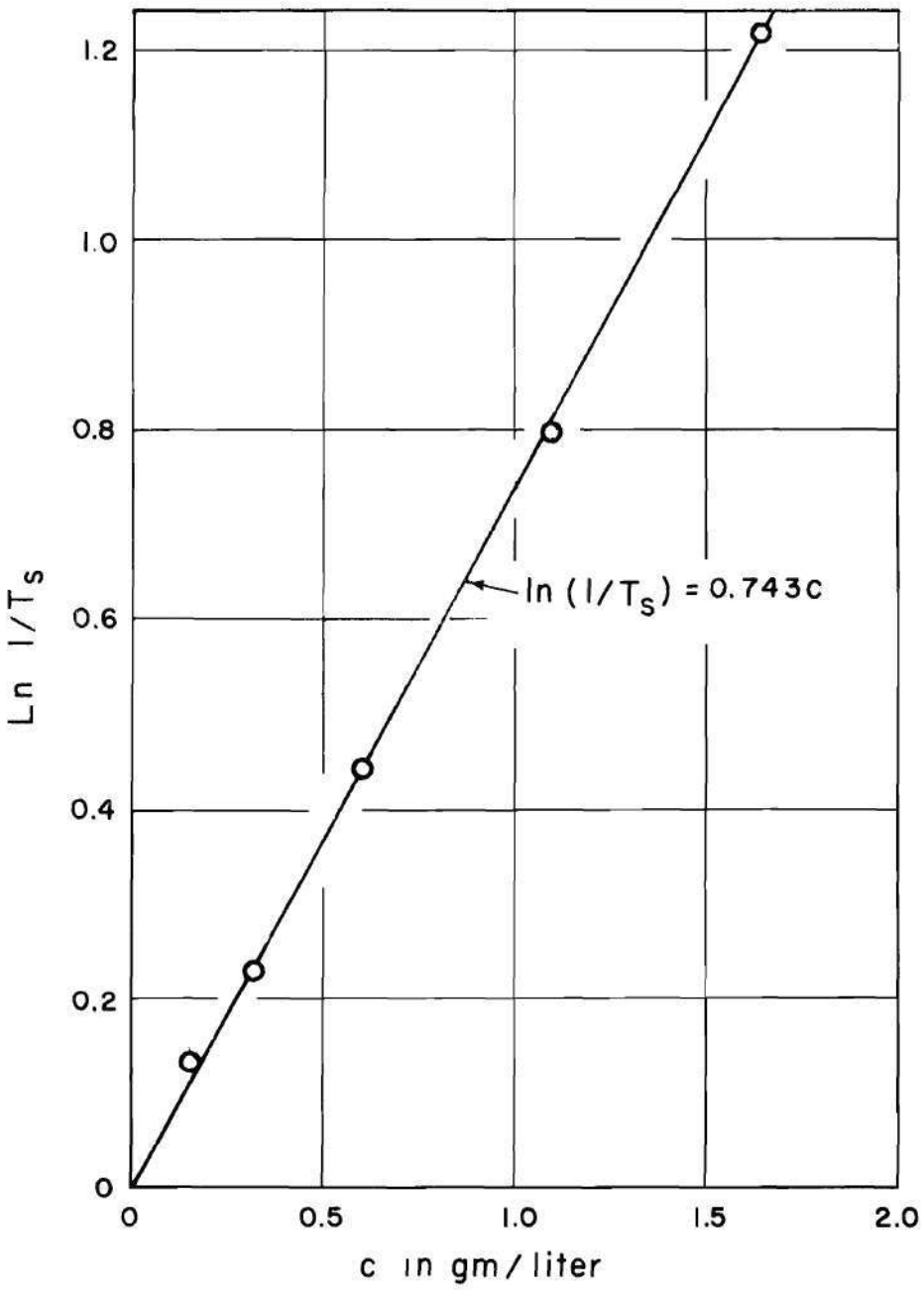

Figure 21. Photospectrometer Calibration.

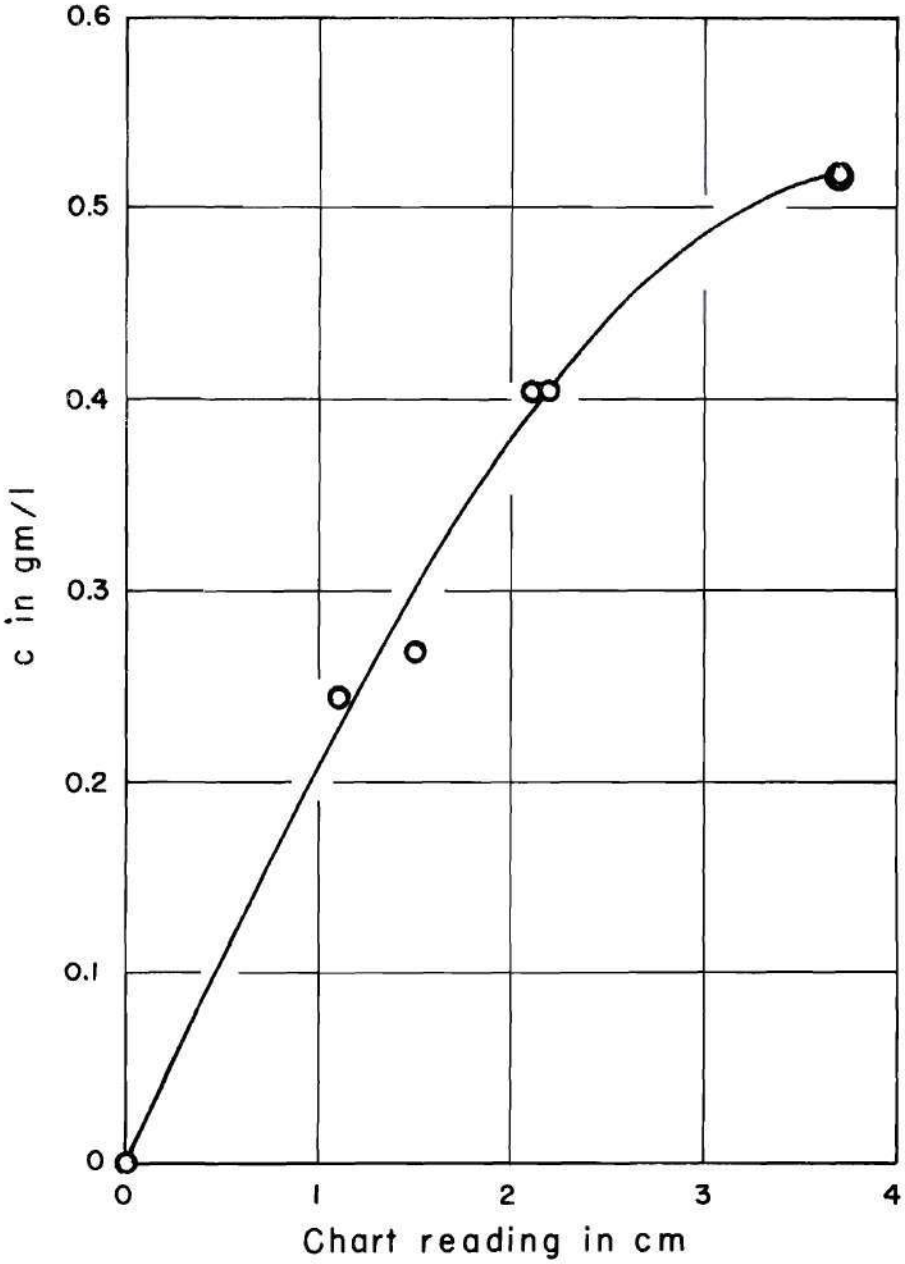

Figure 22. Photocell Calibration.

APPENDIX III

FLUID-DIFFUSION DATA

This section contains data describing the eddy diffusion of fluids.

A typical table of data is presented on page 19. Table 8 contains the data collection in this study.

Table 8. Fluid-Diffusion Data

Run 1

Column: Length of dye injection, LDI; 5.77 cm

Pump: Not recorded, check-run with column tilted.

Chart Reading,* CR (cm)	Concentration, c (gm/l)	Length, L (cm)	100/L (cm^{-1})	ln $c\sqrt{L}$
1.0	0.225	19.8	5.025	0
1.5	0.310	23.7	4.219	0.412
2.0	0.378	30.3	3.300	0.732
2.5	0.430	35.5	2.817	0.940
3.0	0.470	40.3	2.481	1.095
3.5	0.505	46.8	2.137	1.240
4.0	0.536	64.0	1.563	1.458

*Note: The chart reading for a given concentration does not change from run-to-run, so it will be omitted from following tables.

(Continued)

Table 8. Fluid-Diffusion Data

Run 2

Column: Length of dye injection, LDI; 7.66 cm

Pump: Not recorded, check-run with column tilted.

Concentration, c (gm/l)	Length, L (cm)	100/L (cm^{-1})	ln c$\sqrt{L}$
0.225	19.6	5.102	0
0.310	24.5	4.082	0.426
0.378	29.1	3.436	0.712
0.430	32.1	3.115	0.819
0.470	38.0	2.632	1.063
0.505	43.3	2.309	1.200
0.536	49.7	2.012	1.330

Run 3

Column: Length of dye injection, LDI, 8.10 cm

Pump: Not recorded, check-run with column vertical.

Concentration, c (gm/l)	Length, L (cm)	100/L (cm^{-1})	ln c$\sqrt{L}$
0.225	18.3	5.464	-0.0387
0.310	22.3	4.484	0.381
0.378	25.1	3.984	0.640
0.430	27.9	3.584	0.820
0.470	31.9	3.135	0.975
0.505	35.0	2.857	1.095
0.536	40.1	2.494	1.224

(Continued)

Table 8. Fluid-Diffusion Data

Run 4

Column: Length of dye injection, LDI; 3.56 cm. Pressure, P_c; 10 psi

Pump: Amplitude, a_o; 1-1/2 in. Frequency, f; 3 cps. Pressure, P_p; 24 psi. Spring, S; 16 in. Temperature, T; 74°F. Weights, W; 22.

Concentration, c (gm/l)	Length, L (cm)	100/L (cm^{-1})	ln $c\sqrt{L}$
0.225	24.3	4.115	0.104
0.310	27.5	3.636	0.486
0.378	31.2	3.205	0.745
0.430	34.4	2.907	0.924
0.470	37.4	2.667	1.058
0.505	39.9	2.506	1.160
0.536	42.5	2.353	1.251

Run 5

Column: Length of dye injection, LDI; 4.10 cm. Pressure, P_c; 10 psi

Pump: Amplitude, a_o; 3-1/2 in. Frequency, f; 3 cps. Pressure, P_p; 40 psi. Spring, S; 16 in. Temperature, T; 74°F. Weights, W; 22

Chart Reading, CR (cm)	Concentration, c (gm/l)	Length, L (cm)	100/L (cm^{-1})	ln $c\sqrt{L}$
0.5	0.127	15.6	6.41	-0.725
1.0	0.225	24.9	4.02	0.116
1.5	0.310	41.3	2.42	0.690
1.75	0.345	52.1	1.92	0.911

(Continued)

Table 8. Fluid-Diffusion Data

Run 6

Column: Length of dye injection, LDI, 3.20 cm. Pressure, P_c; 10 psi

Pump: Amplitude, a_o; 2-1/2 in. Frequency, f; 4 cps. Pressure, P_p; 64 psi. Spring, S; 16 in. Temperature, T; 75°F. Weights, W; 22.

Concentration, c (gm/l)	Length, L (cm)	100/L (cm^{-1})	ln $c\sqrt{L}$
0.225	11.8	8.47	-0.259
0.310	13.5	7.41	0.131
0.378	14.6	6.85	0.329
0.430	15.9	6.29	0.538
0.470	17.3	5.78	0.670
0.505	18.3	5.46	0.770
0.536	18.8	5.32	0.845

Run 7

Column: Length of dye injection, LDI; 3.75 cm. Pressure, P_c; 10 psi

Pump: Amplitude, a_o; 3-1/2 in. Frequency, f; 4 cps. Pressure, P_p; 60 psi. Spring, S; 16 in. Temperature, T; 75°F. Weights, W; 12.

Concentration, c (gm/l)	Length, L (cm)	100/L (cm^{-1})	ln $c\sqrt{L}$
0.225	8.0	12.50	-0.455
0.310	9.6	10.41	-0.0387
0.378	10.9	9.17	0.272
0.430	11.8	8.47	0.390
0.470	12.8	7.81	0.519
0.505	13.4	7.46	0.615
0.536	14.3	6.99	0.670

(Continued)

Table 8. Fluid-Diffusion Data

Run 8

Column: Length of dye injection, LDI; 5.41 cm. Pressure, P_c; 10 psi

Pump: Amplitude, a_o; 1-1/2 in. Frequency, f; 4 cps. Pressure, P_p; 42 psi. Spring, S; 16 in. Temperature, T; 75°F. Weights, W; 22.

Concentration, c (gm/l)	Length, L (cm)	100/L (cm^{-1})	ln $c\sqrt{L}$
0.225	19.0	5.26	-0.0192
0.310	22.6	4.42	0.388
0.378	25.7	3.89	0.652
0.430	29.3	3.41	0.845
0.470	33.2	3.01	0.995
0.505	37.2	2.69	1.124
0.536	43.6	2.29	1.266

Run 9

Column: Length of dye injection, LDI; 4.19 cm. Pressure, P_c; 10 psi

Pump: Amplitude, a_o; 2 in. Frequency, f; 4 cps. Pressure, P_p; 32 psi. Spring, S; 16 in. Temperature, T; 71°F. Weights, W; 12.

Concentration, c (gm/l)	Length, L (cm)	100/L (cm^{-1})	ln $c\sqrt{L}$
0.225	15.0	6.67	-0.138
0.310	17.3	5.78	0.254
0.378	20.4	4.90	0.534
0.430	22.1	4.52	0.703
0.470	24.2	4.13	0.883
0.505	26.8	3.73	0.963
0.536	28.9	3.46	1.057

(Continued)

Table 8. Fluid-Diffusion Data

Run 10

Column: Length of dye injection, LDI; 4.65 cm. Pressure, P_c; 10 psi

Pump: Amplitude, a_o; 2 in. Frequency, f; 5 cps. Pressure, P_p; 36 psi. Spring, S; 16 in. Temperature, T; 71°F. Weights, W; 0.

Concentration, c (gm/l)	Length, L (cm)	100/L (cm^{-1})	ln $c\sqrt{L}$
0.225	12.7	7.87	-0.223
0.310	14.9	6.71	0.181
0.378	17.7	5.65	0.464
0.430	21.3	4.69	0.688
0.470	23.5	4.26	0.824
0.505	26.9	3.72	0.963
0.536	30.0	3.33	1.078

Run 11

Column: Length of dye injection, LDI; 3.10 cm. Pressure, P_c, 10 psi

Pump: Amplitude, a_o; 2.85 in. Frequency, f; 5 cps. Pressure, P_p; 97 psi. Spring, S; 16 in. Temperature, T; 73°F. Weights, W; 0.

Concentration, c (gm/l)	Length, L (cm)	100/L (cm^{-1})	ln $c\sqrt{L}$
0.225	6.9	14.56	-0.529
0.310	7.9	12.63	-0.136
0.378	9.2	10.86	0.138
0.430	10.3	9.71	0.322
0.470	11.3	8.85	0.457
0.505	12.2	8.20	0.565
0.536	13.5	7.41	0.676

(Continued)

Table 8. Fluid-Diffusion Data

Run 12

Column: Length of dye injection, LDI; 4.37 cm. Pressure, P_c; 10 psi

Pump: Amplitude, a_o; 1.4 in. Frequency, f; 5 cps. Pressure, P_p; 28 psi. Spring, S; 16 in. Temperature, T; 73°F. Weights, W; 0.

Concentration, c (gm/l)	Length, L (cm)	100/L (cm^{-1})	ln $c\sqrt{L}$
0.225	16.9	5.92	-0.0774
0.310	19.4	5.15	0.312
0.378	22.7	4.41	0.587
0.430	25.5	3.92	0.775
0.470	29.3	3.41	0.931
0.505	32.7	3.06	1.060
0.536	36.0	2.78	1.170

Run 13

Column: Length of dye injection, LDI; 4.22 cm. Pressure, P_c; 10 psi

Pump: Amplitude, a_o; 2-1/2 in. Frequency, f; 5 cps. Pressure, P_p; 48 psi. Spring, S; 16 in. Temperature, T; 71°F. Weights, W; 0.

Concentration, c (gm/l)	Length, L (cm)	100/L (cm^{-1})	ln $c\sqrt{L}$
0.225	8.6	11.61	-0.401
0.310	9.8	10.19	-0.0284
0.378	11.1	9.01	0.231
0.430	12.2	8.20	0.405
0.470	13.7	7.30	0.554
0.505	15.3	6.54	0.680
0.536	16.3	6.13	0.772

(Continued)

Table 8. Fluid-Diffusion Data

Run 14

Column: Length of dye injection, LDI; 3.90 cm. Pressure, P_c; 10 psi

Pump: Amplitude, a_o; 2 in. Frequency, f; 3 cps. Pressure, P_p; 30 psi. Spring, S; 16 in. Temperature, T; 73°F. Weights, W; 22.

Concentration, c (gm/l)	Length, L (cm)	100/L (cm^{-1})	ln $c\sqrt{L}$
0.225	22.6	4.42	0.0676
0.310	26.8	3.73	0.473
0.378	30.2	3.31	0.732
0.430	34.4	2.91	0.924
0.470	39.1	2.56	1.078
0.505	44.2	2.26	1.210
0.536	48.0	2.08	1.313

Run 15

Column: Length of dye injection, LDI; 7.36 cm. Pressure, P_c, 10 psi

Pump: Amplitude, a_o; 2-1/2 in. Frequency, f; 2 cps. Pressure, P_p; 32 psi. Spring, S; 18 in. Temperature, T; 73°F. Weights, W; 37.

Concentration, c (gm/l)	Length, L (cm)	100/L (cm^{-1})	ln $c\sqrt{L}$
0.225	25.9	3.86	0.135
0.310	29.5	3.39	0.520
0.378	33.6	2.98	0.785
0.430	36.2	2.76	0.950
0.470	40.6	2.46	1.10
0.505	42.3	2.36	1.19
0.536	45.8	2.18	1.29

(Continued)

Table 8. Fluid-Diffusion Data

Run 16

Column: Length of dye injection, LDI; 4.38 cm. Pressure P_c; 10 psi

Pump: Amplitude, a_o; 3-1/2. Frequency, f; 2 cps. Pressure, P_p; 36 psi. Spring, S; 18. Temperature, T; 73°F. Weights, W; 37.

Concentration, c (gm/l)	Length, L (cm)	100/L (cm^{-1})	ln $c\sqrt{L}$
0.225	22.5	4.44	0.0658
0.310	27.1	3.69	0.479
0.378	31.8	3.14	0.755
0.430	35.8	2.79	0.943
0.470	39.7	2.52	1.084
0.505	42.4	2.36	1.190
0.536	46.9	2.13	1.30

Run 17

Column: Length of dye injection, LDI; 3.72 cm. Pressure P_c; 10 psi

Pump: Amplitude, a_o; 2 in. Frequency, f; 2 cps. Pressure, P_p; 28 psi. Spring, S; 18 in. Temperature, T; 73°F. Weights, W; 37.

Chart Reading, CR (cm)	Concentration, c (gm/l)	Length, L (cm)	100/L (cm^{-1})	ln $c\sqrt{L}$
0.5	0.127	36.6	2.73	-0.263
1.0	0.225	57.2	1.75	0.530
1.5	0.310	83.9	1.19	1.043
1.75	0.345	105.4	0.952	1.262
2.0	0.378	126.3	0.794	1.450

(Continued)

Table 8. Fluid-Diffusion Data

Run 18

Column: Length of dye injection, LDI; 2.75 cm. Pressure, P_c; 10 psi

Pump: Amplitude, a_o; 3-1/2 in. Frequency, f; 3 cps. Pressure, P_p; 44 psi. Spring, S; 16 in. Temperature, T; 70°F. Weights, W; 22.

Concentration, c (gm/l)	Length, L (cm)	100/L (cm^{-1})	ln $c\sqrt{L}$
0.225	12.0	8.93	-0.249
0.310	14.4	6.94	0.161
0.378	16.4	6.10	0.425
0.430	18.1	5.52	0.604
0.470	20.1	4.98	0.745
0.505	22.2	4.50	0.866
0.536	24.2	4.13	0.970

Run 19

Column: Length of dye injection, LDI; 3.77 cm. Pressure, P_c; 10 psi

Pump: Amplitude, a_o; 2-1/2 in. Frequency, f; 4 cps. Pressure, P_p; 40 psi. Spring, S; 16 in. Temperature, T; 70°F. Weights, W; 12.

Concentration, c (gm/l)	Length, L (cm)	100/L (cm^{-1})	ln $c\sqrt{L}$
0.225	12.7	7.87	-0.220
0.310	15.4	6.49	0.195
0.378	17.5	5.71	0.458
0.430	20.1	4.98	0.656
0.470	21.6	4.63	0.783
0.505	24.5	4.08	0.915
0.536	26.9	3.72	1.020

(Continued)

Table 8. Fluid-Diffusion Data

Run 20

Column: Length of dye injection, LDI; 3.50 cm. Pressure P_c; 10 psi

Pump: Amplitude, a_o; 0.95 in. Frequency, f; 5 cps. Pressure, P_p; 22 psi. Spring, S; 16 in. Temperature, T; 77°F. Weights, W; 22.

Chart Reading, CR (cm)	Concentration, c (gm/l)	Length, L (cm)	100/L (cm^{-1})	ln $c\sqrt{L}$
0.5	0.127	22.2	4.50	-0.515
1.0	0.225	31.0	3.23	0.225
1.5	0.310	39.4	2.59	0.665
2.0	0.378	50.7	1.97	0.990
2.4	0.420	72.5	1.38	1.275

Run 21

Column: Length of dye injection, LDI; 2.80 cm. Pressure, P_c; 10 psi

Pump: Amplitude, a_o; 1.6 in. Frequency, f; 4 cps. Pressure, P_p; 24 psi. Spring, S; 16 in. Weights, W; 12.

Concentration, c (gm/l)	Length, L (cm)	100/L (cm^{-1})	ln $c\sqrt{L}$
0.127	20.1	4.98	-0.565
0.225	28.8	3.47	0.189
0.310	38.5	2.60	0.652
0.378	50.6	1.98	0.990
0.430	69.4	1.44	1.275

(Continued)

Table 8. Fluid-Diffusion Data

Run 22

Column: Length of dye injection, LDI; 6.30 cm. Pressure, P_c; 10 psi

Pump: Amplitude, a_o; 1.95 in. Frequency, f; 2 cps. Pressure, P_p; 25 psi. Spring, S; 18 in. Weights, W; 37.

Concentration, c (gm/l)	Length, L (cm)	100/L (cm^{-1})	ln $c\sqrt{L}$
0.225	38.0	2.63	0.326
0.310	44.6	2.24	0.710
0.378	51.8	1.93	1.00
0.430	58.3	1.72	1.187
0.470	66.8	1.50	1.346
0.505	74.1	1.35	1.470
0.536	87.8	1.13	1.615

Run 23

Column: Length of dye injection, LDI; 4.70 cm. Pressure, P_c; 10 psi

Pump: Amplitude, a_o; 1.4 in. Frequency, f; 3 cps.

Concentration, c (gm/l)	Length, L (cm)	100/L (cm^{-1})	ln $c\sqrt{L}$
0.127	34.9	2.87	-0.289
0.225	55.9	1.79	0.519
0.305	96.6	1.04	1.10

APPENDIX IV

PHOTOMICROGRAPH AND FALL VELOCITY OF BEADS

The diameters of the sieved fraction of beads used in this study were measured by scaling the diameters of one hundred of the beads shown in the photomicrograph (Fig. 23). The mean diameter obtained was 0.01168 in with an estimated standard deviation of 0.00060 in.

The fall velocities of these beads were measured by timing the fall of each of one hundred beads through a distance of 0.902 ft. A few measurements made at 0.451 ft showed that the distances were sufficient to make acceleration effects negligible. The mean time of fall was 24.50 sec with an estimated standard deviation of 1.88 sec; therefore, the mean fall velocity was 0.0368 ft per sec. This fall velocity and diameter correspond to a density of 2.54 slugs per cubic ft. The measurements were made in still water at 71°F.

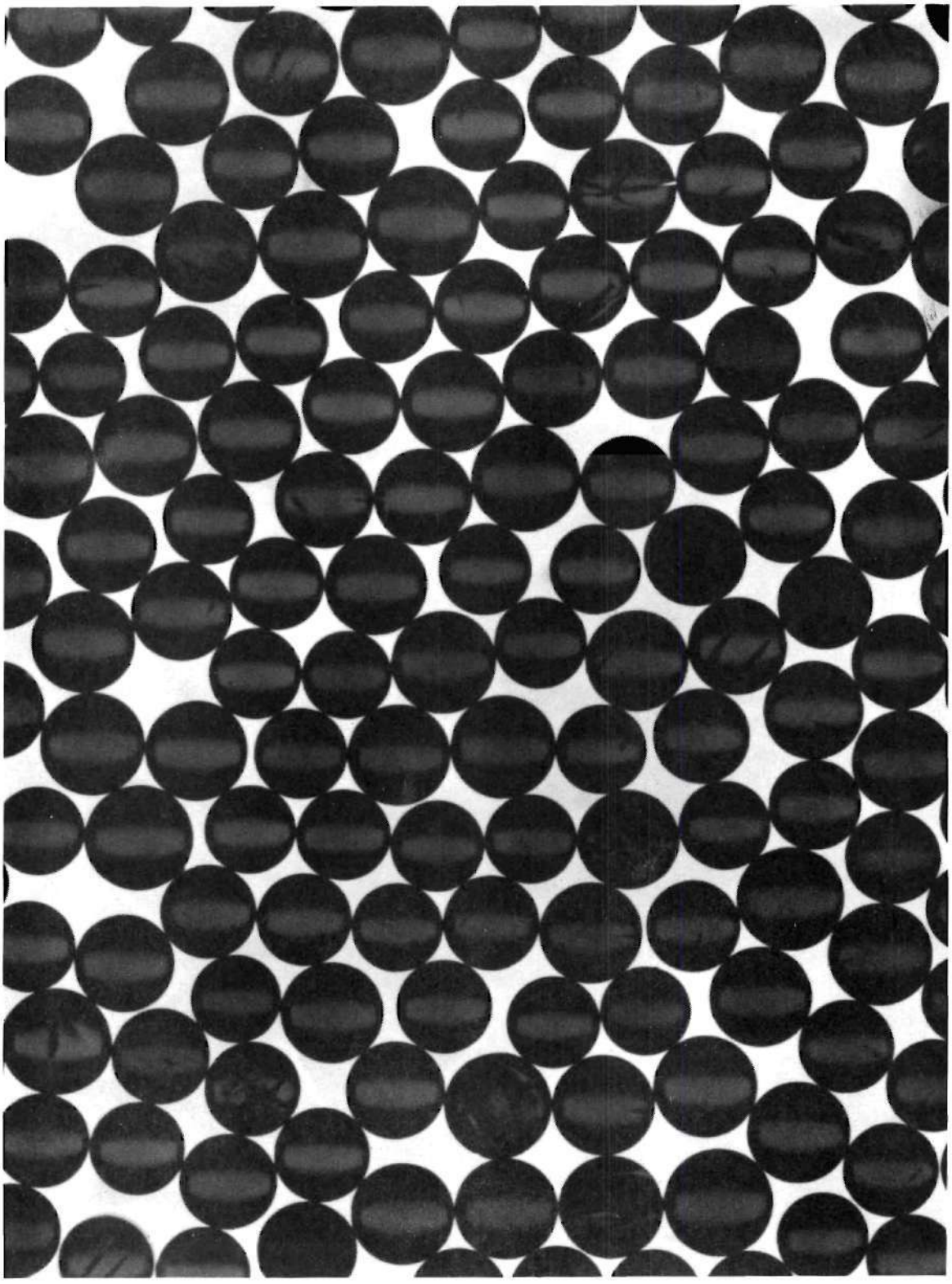

Figure 23. Microphotograph of Particles (50X).

APPENDIX V

PARTICLE DIFFUSION DATA

This section contains data describing the eddy diffusion of ion-exchange resin beads.

A typical table of data is described on page 41. Table 9 contains the data collected in this study.

Table 9. Particle-Diffusion Data

Runs T and X

Column	T	X	Counter	T X	Pump	T	X
Top	43.615	43.650	High Volt.	1100	Amplitude	2"	
Bottom	30.655	30.680	Gain	8 x 1	Frequency	2 cps	
Pressure	9	9	Bandwidth	0.5 mc	Pressure	23 psi	23 psi
			Δ e	10	Springs	8	10
z^*	17.30	17.32			Weights	All	All
					Temp.	78°	70°

z^* (cm)	e	R	$z-z^*$	C(counts/min)	Remarks
19.450	24.5	205-11/7	2.15	1876	T
20.765	24.5	186-57/14	3.47	854	
22.00	24.5	160-2/18	4.70	569	(without
23.385	24.5	73-54/10	6.09	473	lead in
21.300	24.5	169-39/16	4.00	678	slit)
20.110	24	168-35/9	2.81	1199	
19.425	24.5	187-0/9	2.11	1330	X
20.670	24.5	172-48/14	3.35	790	
22.080	24.5	186-8/21	4.76	567	(with lead
23.160	24.5	155-22/20	5.84	497	in slit)
21.130	24.5	157-37/15	3.81	672	
19.950	24.5	128-8/7m 52.7s	2.63	1041	

(Continued)

Table 9. Particle Diffusion Data

Runs S and V

Column	S	V	Counter	S & V	Pump	S	V
Top	43.580	43.655	High Volt.	1100	Amplitude	2-1/2"	
Bottom	30.645	30.680	Gain	8 x 1	Frequency	2 cps	
Pressure	9 psi	9 psi	Bandwidth	0.5 mc	Springs	8	
$(\sin \alpha)^{-1}$	4.372		Δ e	10	Pressure	25 psi	26 psi
z^*	17.29	17.32			Weights	All	All
					Temp.	76°	74°

z^* (cm)	e	R	$z-z^*$	C(counts/min)	Remarks
19.420	24.5	278-19/8	2.13	2226	S
20.620	24.5	175-14/10	3.33	1121	
19.990	24.5	192-63/8	2.70	1544	(without lead
21.440	24.5	174-52/14	4.15	799	in slit)
22.345	24.5	179-49/20	5.06	575	
24.110	24.5	70-19/10	6.82	450	After 122
19.450	24.5	197-21/6	2.16	2105	pump stalled
19.415	24.5	190-17/9	2.10	1353	V
19.415	24.5	95-20/45	2.10	1355	
20.645	24.5	189-33/14	3.33	866	(with lead
21.845	24.5	179-10/18	4.53	637	in slit)
23.270	24.5	159-55/20	5.95	512	
21.290	24.5	145-24/13m 6s	3.97	712	

(Continued)

Table 9. Particle-Diffusion Data, Runs U & W

Column	U	W	Counter	U & W	Pump	U	W
Top	43.615	43.655	High Voltage	1100	Amplitude	3-1/2"	
Bottom	30.655	30.680	Gain	8 x 1	Frequency	2 cps	
Pressure	9	9	Bandwidth	0.5 mc	Pressure	35 psi	32 psi
z^*	17.30	17.32	Δe	10	Springs	8	8
					Weights	All	All
					Temp.	78°	74°

z (cm)	e	R	$z-z^*$	C(counts/min)	Remarks
19.540	24	186-7/6	2.24	1985	U
20.660	24	176-11/9	3.36	1253	
21.960	24	180-16/14	4.66	824	(without
23.220	24	176-47/18	5.92	628	lead in
24.495	24	183-63/22	7.20	535	slit)
25.645	24	76-29/10	8.35	489	
20.060	24	146-38/6m 17s	2.76	1493	
19.540	24.5	190-58/10	2.22	1222	W
20.700	24	194-19/14	3.38	888	
21.985	24	182-5/17	4.67	685	(with lead
23.350	24	165-31/19	6.03	557	in slit)
24.710	24	155-13/20	7.39	497	
21.280	24	173-16/19	3.96	792	
20.060	24.5	166-57/10	2.74	1068	

(Continued)

Table 9. Particle-Diffusion Data

Runs O and Q

Column	O	Q	Counter	O & Q	Pump	O	Q
Top	43.600	43.610	High Volt.	1100	Amplitude	2"	
Bottom	30.640	30.645	Gain	8 x 1	Frequency	3 cps	
Pressure	9	9	Bandwidth	0.5 mc	Springs	16	16
$(\sin \alpha)^{-1}$	4.362	4.362	Δ e	10	Weights	28	28
z^*	17.28	17.29			Pressure	37 psi	37 psi
					Temp.	72°	72°

z (cm)	e	R	$z-z^*$	C(counts/min)	Remarks
19.540	24.5	203-5/9	2.26	1444	O
20.650	24.5	177-34/12	3.37	947	
22.640	24.5	202-63/20	4.76	650	(with lead
23.500	24.5	175-47/23	6.22	489	in slit)
24.950	24.5	174-30/26	7.67	430	
20.090	24.5	186-51/10	2.81	1196	
21.290	24.5	106-19/8m 38s			
19.440	24.5	193-54/5	2.15	2481	Q
20.795	24.5	200-22/10	3.51	1283	
22.170	24.5	170-37/15	4.88	728	(without
23.470	24.5	173-2/20	6.18	554	lead in
24.810	24.5	29-5/4	7.52	465	slit)
20.100	24.5	133-13/5	2.81	1705	

(Continued)

Table 9. Particle-Diffusion Data

Runs H and Y

Column	H	Y	Counter	H & Y	Pump	H	Y
Top	43.575	43.645	High Volt.	1100	Amplitude	2-1/2"	
Bottom	30.695	30.685	Gain	8 x 1	Frequency	3 cps	
Pressure	9	9	Bandwidth	0.5 mc	Springs	16	16
$(\sin \alpha)^{-1}$	4.388	4.37	Δ e	10	Weights	28	28
z^*	17.34	17.33		78	Pressure	44 psi	45 psi
					Temp.	73°	68°

z^* (cm)	e	R	$z-z^*$	C(counts/min)	Remarks
19.590	25	169-0/8	2.25	1274	H
20.480	24.5	190-9/11	3.14	1028	
21.680	25	196-40/16	4.34	709	(with lead
22.920	24.5	203-15/21	5.58	541	in slit)
24.370	24.5	184-4/23	7.03	434	
25.720	24.5	201-1/29	8.38	366	
19.500	24.5	196-17/49	2.17	1318	
19.460	24.5	174-52/9	2.13	1243	Y
20.600	24.5	182-37/12	3.27	974	
21.740	24.5	175-63/15	4.41	750	(without
19.455	24.5	182-26/6	2.13	1947	lead in
20.620	24.5	181-54/9	3.29	1293	slit)
22.290	24.5	166-23/14	4.96	762	

(Continued)

Table 9. Particle-Diffusion Data

Runs A and B

Column	A	B	Counter	A & B	Pump	A	B
Top	43.590	43.590	High Volt.	1100	Amplitude	2-1/2"	
Bottom	30.670	30.670	Gain	8 x 1	Frequency	3 cps	
Pressure	9	9	Bandwidth	0.5 mc	Springs	16	16
$(\sin \alpha)^{-1}$	4.374		Δ e	10	Weights	28	28
z^*	17.31				Pressure		
					Temp.	81°	76°

z^* (cm)	e	R	$z-z^*$	C(counts/min)	Remarks
21.050	23.5	205-16/10	3.74	1235	A
22.195	23.5	234-35/16	4.89	860	
23.380	23.5	206-50/19	6.07	619	
24.470	23.5	205-15/22	7.16	519	
19.910	25.5	200-40/7	2.60	1756	
21.140	25.5	176-45/9	3.83	1171	
21.140	25.5	197-49/10	3.83	1188	B
22.300	25.5	198-61/14	4.99	832	
23.840	25.5	205-50/20	6.53	581	
25.410	25.5	180-26/22	8.10	445	
26.965	25.5	205-9/30	9.66	360	
28.310	25.5	205-19/32	11.00	333	
22.460	26	115-4/8.958	5.15	807	

(Continued)

Table 9. Particle-Diffusion Data

Runs D and F

Column	D	F	Counter	D & F	Pump	D	F
Top	43.610	43.585	High Volt.	1100	Amplitude	3-1/2"	
Bottom	30.680	30.690	Gain	8 x 1	Frequency	3 cps	
Pressure	9	9	Bandwidth	0.5 mc	Springs	16	16
$(\sin \alpha)^{-1}$	4.374	4.382	Δ e	10	Weights	28	32
z^*	17.32	17.33			Pressure	67 psi	57 psi
					Temp.	75°	75°

z^* (cm)	e	R	z-z*	C(counts/min)	Remarks
19.575	25	169-21/9	2.26	1126	(with lead
20.660	25	203-20/13	3.34	923	in slit)
22.055	25	206-3/17	4.74	698	
23.430	25	199-36/28	6.21	561	D
24.730	25	218-23/25	7.41	481	
26.215	25	188-45/25	8.90	405	
28.040	25	196-8/30	10.72	340	
22.530	25	190-12/17	5.21	638	
19.680	22.5	217-59/7	2.35	1992	F
20.860	22.5	229-14/10	3.53	1467	
22.170	22.5	204-36/12	4.84	1090	
23.500	22.5	204-49/14	6.17	936	
24.880	22.5	174-44/16	7.55	699	
26.318	22.5	185-14/21	8.98	564	
28.280	22.5	159-8/22	10.95	463	
21.310	22.5	206-30/10	3.98	1321	

(Continued)

Table 9. Particle-Diffusion Data

Runs C and E

Column	C	E	Counter	C & E	Pump	C	E
Top	43.615	43.600	High Volt.	1100	Amplitude	1-1/2"	
Bottom	30.655	30.680	Gain	8 x 1	Frequency	3 cps	
Pressure	9	9	Bandwidth	0.5 mc	Springs	16	
$(\sin \alpha)^{-1}$		4.374	Δe	10	Weights	30	28
z^*	17.30	17.32			Pressure	32 psi	
					Temp.	75°	74°

z^* (cm)	e	R	z-z*	C(counts/min)	Remarks
19.200	25	202-53/10	1.88	1298	C
20.890	25	217-33/17	3.57	819	
22.240	25	199-59/23	4.92	556	(with lead
23.600	25	209-56/29	6.28	463	in slit)
24.880	25	55-39/8	7.56	445	
22.065	25	134-45/15	4.75	575	
19.370	22	232-38/6	2.04	2481	E
20.400	22	217-40/10	3.07	1393	
21.280	22	194-5/14	3.95	887	(without
22.300	22	190-46/20	4.97	610	lead in
26.780	22	261-29/40	9.45	418	slit)
23.715	22	193-1/25	6.39	494	
25.085	22	228-32/32	7.76	457	
28.120	22	219-0/35	10.79	400	
21.400	22	215-4/15	4.07	918	

(Continued)

Table 9. Particle-Diffusion Data

Runs J and L

Column	J	L	Counter	J & L	Pump	J	L
Top	43.520	43.590	High Volt.	1100	Amplitude	1-1/2"	
Bottom	30.610	30.630	Gain	8 x 1	Frequency	4 cps	
Pressure	9	9	Bandwidth	0.5 mc	Springs	16	
$(\sin \alpha)^{-1}$	4.379	4.362	Δ e	10	Weights	28	
z*	17.25	17.27			Pressure	22 psi	24 psi
					Temp.	74°	78°

z* (cm)	e	R	z-z*	C(counts/min)	Remarks
19.460	24.5	208-16/9	2.21	1481	J
20.575	24.5	201-30/13	3.33	992	
21.740	24.5	169-38/16	4.49	678	(with lead
22.980	24.5	164-26/20	5.73	526	in slit)
26.730	24.5	265-44/425	9.48	400	
24.320	24.5	240-12/33	7.07	466	
19.970	24.5	200-68/11	2.72	1216	
19.455	25	229-17/6	2.19	2446	L
20.530	25	215-24/10	3.26	1378	
21.790	25	184-1/15	4.52	785	(without
23.100	25	173-12/20	5.83	554	lead in
24.480	25	56-19/8	7.21	450	slit)
19.940	25	173-0/6	2.67	1847	

(Continued)

Table 9. Particle-Diffusion Data

Runs P and R

Column	P	R	Counter	P & R	Pump	P	R
Top	43.600	43.600	High Volt.	1100	Amplitude	2"	
Bottom	30.645	30.645	Gain	8 x 1	Frequency	4 cps	
Pressure	9	9	Bandwidth	0.5 mc	Springs	16	
$(\sin \alpha)^{-1}$	4.37	4.37	Δ e	10	Weights	28	28
z^*	17.29	17.29			Pressure	26 psi	23 psi
					Temp.	73°	74°

z^* (cm)	e	R	z-z*	C(counts/min)	Remarks
19.385	24.5	199-16/9	2.10	1417	P
20.685	24.5	205-59/13	3.40	1014	
22.040	24.5	190-26/17	4.75	717	(with lead
23.540	24.5	68-22/8m3s	6.25	545	in slit)
23.540	24.5	101-27/12	6.25	541	
25.100	24.5	35-45/5.077	7.81	450	
20.040	24.5	172-7/9	2.75	1224	
19.480	24.5	189-58/5	2.19	2430	R
20.680	24.5	190-60/8	3.39	1528	
22.215	24.5	189-41/14	4.93	867	(without
23.720	24.5	182-50/19	6.43	616	lead in
25.210	24.5	166-62/22	7.92	486	slit)
20.010	24.5	231-63/8	2.72	1856	
21.340	24.5	200-8/11	4.05	1164	

(Continued)

Table 9. Particle-Diffusion Data

Runs I and G

Column	I	G	Counter	I & G	Pump	I	G
Top	43.57	43.580	High Volt.	1100	Amplitude	2-1/2"	
Bottom	30.680	30.685	Gain	8 x 1	Frequency	4 cps	
Pressure	9	9	Bandwidth	85 mc	Springs	16	
$(\sin \alpha)^{-1}$	4.386	4.306	Δ e	10	Weights	28	
z*	17.32	17.33			Pressure	34 psi	33 psi
					Temp.	76°	74°

z* (cm)	e	R	z-z*	C(counts/min	Remarks
19.500	24.5	201-33/10	2.18	1212	I
20.480	24.5	199-27/12	3.16	1064	
21.650	24.5	210-18/16	4.33	841	(with lead
23.040	24.5	205-41/20	5.72	658	in slit)
27.630	24.5	258-1/39	10.31	420	
24.525	24.5	167-20/22	7.21	487	
25.960	24.5	210-43/28	8.64	482	
19.620	22.5	199-13/6	2.29	2125	G
20.625	22.5	227-59/9	3.30	1621	
22.120	22.5	206-2/12	4.79	1099	
23.480	22.5	205-1/16	6.15	820	
28.160	22.5	203-24/48	10.93	453	
25.020	22.5	198-19/20	7.63	634	
26.500	22.5	182-52/22	8.17	532	
21.200	22.5	210-41/10	3.87	1348	

(Continued)

Table 9. Particle-Diffusion Data

Runs K and α

Column	K	α	Counter	K & α	Pump	K	α
Top	43.57	43.590	High Volt.	1100	Amplitude	3-1/2"	
Bottom	30.61	30.620	Gain	8 x 1	Frequency	4 cps	
Pressure	9	9	Bandwidth	0.5 mc	Springs	16	18
$(\sin \alpha)^{-1}$	4.362		Δ e	10	Weights	28	None
z*	17.25	17.26			Pressure	42 psi	
					Temp.	79°	77°

z* (cm)	e	R	z-z*	C(counts/min)	Remarks
19.315	25	201-41/11	2.07	1173	K
19.300	25	199-38/11	2.05	1161	
19.330	25	202-58/11	2.08	1181	(with lead
20.460	25	187-26/12	3.21	1000	in slit)
21.715	25	209-45/16	4.47	839	
23.180	25	199-52/19	5.93	673	
24.360	24	189-43/20	7.11	607	
25.530	25	188-55/23	8.28	526	
19.405	24.5	179-17/8	2.15	1434	α
20.580	24.5	183-35/10	3.32	1175	
21.820	24.5	181-2/12	4.56	965.5	(without
22.970	24.5	202-13/16	5.71	808.8	lead in
24.195	24.5	193-31/18	6.94	687.9	slit)
25.530	24.5	120-7/13	8.27	591.3	
20.020	24.5	158-51/8	2.76	1270	

(Continued)

Table 9. Particle-Diffusion Data

Runs M and N

Column	M	N	Counter	M & N	Pump	M	N
Top	43.610	43.610	High Volt.	1100	Amplitude	1-1/2"	
Bottom	30.640	30.640	Gain	8 x 1	Frequency	5 cps	
Pressure	9	9	Bandwidth	0.5 mc	Springs	16	
$(\sin \alpha)^{-1}$	4.359	4.359	Δ e	10	Weights	None	
z*	17.28	17.28			Pressure	35 psi	
					Temp.	74°	75°

z* (cm)	e	R	z-z*	C(counts/min)	Remarks
19.510	25	225-58/6	2.23	2410	M
20.640	25	197-55/8	3.36	1583	
22.030	25	206-29/14	4.75	944	(without lead
23.440	25	191-49/20	6.16	614	in slit)
24.620	25	157-18/24	7.34	419	
21.120	25	167-52/9	3.84	1193	
20.040	25	210-6/7	2.76	1921	
20.040	24	198-83/10	2.76	1269	N
19.300	24.5	190-60/8	2.02	1528	
20.560	24.5	167-44/10	3.28	1073	(with lead
21.780	24.5	163-10/14	4.50	749	in slit)
23.195	24.5	169-24/20	5.92	542	
24.535	24.5	178-54/25	7.26	458	
21.120	24.5	26-59/1m 55.5s	3.84	892	

(Continued)

Table 9. Particle-Diffusion Data

Runs Y and Δ

Column	Y	Δ	Counter	Y & Δ	Pump	Y	Δ
Top	43.620	43.620	High Volt.	1100	Amplitude	2"	
Bottom	30.620	30.620	Gain	8 x 1	Frequency	5 cps	
Pressure	9	9	Bandwidth	0.5 mc	Springs	16	
z^*	17.26	17.26	Δ e	10	Weights	None	
					Pressure	28 psi	29 psi
					Temp.	74°	76°

z^* (cm)	e	R	$z-z^*$	C(counts/min)	Remarks
19.470	24.5	203-32/8	2.21	1628	Y
20.575	24.5	195-16/10	3.32	1250	
21.820	24.5	175-44/12	4.56	937.0	(without
23.065	24.5	162-33/14	5.81	742.9	lead in
24.180	24.5	154-46/16	6.92	618.9	slit)
20.000	24.5	195-16/9	2.74	1388	
20.000	24.5	173-2/11	2.74	1007	Δ
19.410	24.5	170-60/10	2.15	1094	
20.840	24.5	179-29/13	3.58	883.5	(with lead
22.100	24.5	167-43/15	4.84	715.4	in slit)
23.310	24.5	160-40/17	6.05	604.7	
24.380	24.5	165-50/20	7.12	530.5	
21.470	24.5	160-19/13	4.21	789.2	

(Continued)

Table 9. Particle-Diffusion Data

Columns β and φ

Column	β	φ	Counter	β & φ	Pump	β	φ
Top	43.610	43.620	High Volt.	1100	Amplitude	2-1/2"	
Bottom	30.620	30.620	Gain	8 x 1	Frequency	5 cps	
Pressure	9	9	Bandwidth	0.5 mc	Springs	16	
z^*	17.26	17.26	Δ e	10	Weights	None	
					Pressure	35 psi	36-33 psi
					Temp.	78°	78°

z^* (cm)	e	R	z-z^*	C(counts/min)	Remarks
19.380	24.5	209-23/9	2.12	1489	β
20.620	24.5	188-22/10	3.36	1205	
21.820	24.5	180-8/12	4.56	960.7	(without lead
22.970	24.5	179-58/14	5.71	822.4	in slit)
24.160	24.5	170-29/16	6.90	681.8	
25.290	24.5	170-58/18	8.03	607.7	
19.930	24.5	182-12/9	2.67	1296	
19.380	25.5	163-16/10	2.12	1045	φ
20.750	25.5	162-44/12	3.49	867.7	
21.980	25.5	183-59/16	4.72	735.7	(with lead
23.040	25.5	174-27/17	5.78	656.6	in slit)
24.220	25.5	162-49/18	6.96	578.7	
25.300	25.5	164-7/20	8.04	526.2	
20.040	25.5	162-32/11	2.78	945.5	

(Continued)

Table 9. Particle-Diffusion Data

Columns Φ and Ω

Column	Φ	Ω	Counter	Φ & Ω	Pump	Φ	Ω
Top	43.610	43.610	High Volt.	1100	Amplitude	3"	
Bottom	30.610	30.610	Gain	8 x 1	Frequency	5 cps	
Pressure	9	9	Bandwidth	0.5 mc	Springs	16	
z*	17.25	17.25	Δ e	10	Weights	None	
					Pressure	43 psi	44 psi
					Temp.	73°	77°

z* (cm)	e	R	z-z*	C(counts/min)	Remarks
19.430	24.5	166-35/11	2.18	969.0	Φ
20.670	24.5	171-35/13	3.42	844.5	
21.780	24.5	173-47/15	4.53	741.3	(with lead
23.000	24.5	163-37/16	5.75	654.3	in slit)
24.130	24.5	165-25/18	6.88	588.1	
25.180	24.5	162-0/19	7.93	545.7	
20.025	24.5	168-35/12	2.78	898.9	
19.415	24.5	182-32/9	2.17	1298	Ω
20.660	24.5	165-42/10	3.41	1060	
21.760	24.5	169-20/12	4.51	903.0	(without
23.070	24.5	160-44/13	5.82	791.1	lead in
24.370	24.5	160-18/15	7.12	683.5	slit)
25.480	24.5	160-62/17	8.23	606.0	
20.000	24.5	160-31/9	2.75	1141	

LITERATURE CITED

1. Ismail, H. M., "Turbulent Transfer Mechanism and Suspended Sediment in Closed Channels," Trans. ASCE, 117, p. 409 (1952).

2. Vanoni, V. A., "Transportation of Suspended Sediment by Water," Trans. ASCE, 111, p. 67 (1946).

3. Longwell, J. P. and Malcolm Weiss, "Mixing and Distribution of Liquids in High-Velocity Air Streams," I.E.C., 45, p. 667 (1953).

4. Friedlander, S. K. and H. F. Johnstone, "Deposition of Suspended Particles from Turbulent Gas Streams, I.E.C., 49, p. 1151,

5. Tchen, C. M., Mean Value and Correlation Problems Connected with the Motion of Small Particles Suspended in a Turbulent Fluid, Martinus Nijhoff, The Hague (1947).

6. Peskin, R. L., "Some Effects of Particle-Particle and Particle-Fluid Interaction in Two Phase Flow Systems," Proceedings of the Heat Transfer and Fluid Mechanics Institute, p. 192, Stanford (1960).

7. Lumley, J. L., Some Problems Connected with the Motion of Small Particles in Turbulent Fluid, Ph.D. Thesis, Johns Hopkins University, Baltimore (1957).

8. Corrsin, S. and J. L. Lumley, "On the Equation of Motion for a Particle in Turbulent Fluid," Applied Scientific Research, 6A, p. 114, (1956).

9. Hinze, J. O., Turbulence, McGraw-Hill Book Company, Inc., New York (1959).

10. Torobin, L. B. and W. H. Gauvin, "Fundamental Aspects of Solids-Gas Flow," Canadian Journal of Chemical Engineering, Part I, 37, p. 129 (1959); Part II, id., p. 167 (1959); Part III, id., p. 224 (1959); Part IV, 38, p. 142 (1960); Part V, id. p. 182 (1960); Part VI, 39, p. 113 (1961).

11. Rouse, H., "Mechanics of Sediment Suspension," Proceedings of the Fifth Internation Congress of Applied Mechanics, p. 550, John Wiley and Sons, Inc., New York (1939).

12. Bouwman, J. J., "Opwekking van kunstmatige turbulentie," Laboratorium voor Aero-en Hydrodynamica der Technishe Hogeschool te Delft, technical note (1943).

13. Richardson, L. F., "Some Measurements of Atmospheric Turbulence, Philosophical Transactions, Royal Society of London, 221, Series A, p. 1 (1920).

14. Kolmogoroff, A., "The Local Structure of Turbulence in Incompressible Viscous Fluid for Very Large Reynolds' Numbers," Turbulence, Classic Papers on Statistical Theory, p. 151, Interscience Publishers, Inc., New York (1961).

15. Batchelor, G. K., "Diffusion in a Field of Homogeneous Turbulence. II. The Relative Motion of Particles," Proceedings Cambridge Philosophical Society, 48, p. 345 (1952).

16. Orlob, G. T., "Eddy Diffusion in Homogenous Turbulence," Trans. ASCE, 126, I, p. 397 (1961).

17. Taylor, G. I., "The Dispersion of Matter in Turbulent Flow Through a Pipe," Proceedings of the Royal Society, 223, Series A, p. 446 (1954).

18. Ferrell, J. K., Frances M. Richardson, and K. O. Beatty, Jr., "Dye Displacement Technique for Velocity Distribution Measurements," I.E.C., 47, p. 29 (1955).

19. Eagleson, P. S. and R. G. Dean, "Wave-Induced Motion on Bottom Sediment Particles," Trans. ASCE, 126, I, p. 1162 (1961).

20. Kinsman, S., Radiological Health Handbook, p. 142, Public Health Service (1957).

21. Brush, L. M., Jr., Private communication.

22. Torobin, L. B. and W. H. Gauvin, "The Drag Coefficients of Simple Spheres Moving in Steady and Accelerated Motion in a Turbulent Fluid," Journ. AICh. E., Vol. 7, No. 4, p. 615 (1961).

23. Carstens, M. R., "Accelerated Motion of a Spherical Particle," Transactions, American Geophysical Union, Vol. 33, No. 5, p. 713 (1952).